

Chapter 2

Composition, Formation, and Occurrence of Polymetallic Nodules

T. Kuhn, A. Wegorzewski, C. Rühlemann, and A. Vink

Abstract Manganese nodules occur as two-dimensional deposits in abyssal plains of all major oceans. In the Clarion-Clipperton Zone of the northeast equatorial Pacific alone, the amount of nodules is estimated to 21 billion tons indicating the huge potential of this deposit type. Apart from manganese, metals of economic interest are nickel, copper, and cobalt, but the nodules also contain interesting amounts of molybdenum, titanium, lithium, and the rare earth elements. Therefore they are also called as polymetallic nodules.

The nodules consist of concentrically banded zones of micro-layers around a nucleus. They form by metal precipitation either from the ambient seawater (hydrogenetic) or from pore water in the sediments (diagenetic). They generally consist of a mixture of both genetic types but in varying proportions. Hydrogenetic precipitation leads to the enrichment of other metals than diagenetic precipitation (cobalt, rare earths versus nickel, copper, etc.), thus controlling the general chemical composition of the nodules. It seems that suboxic conditions (dissolved oxygen content is less than 5% of the saturation concentration) are generally necessary for diagenetic formation and oxic conditions for hydrogenetic formation. The change from oxic to suboxic conditions and vice versa is probably climatically controlled.

Manganese nodules from the sediment surface are mainly composed of phyllo-manganates such as vernadite, birnessite, and buserite, whereas amounts of todorokite seem to be negligible. Phyllomanganates contain their metals either as substitutes of manganese in octahedral layers or as hydrated cations in the interlayers.

Well-studied occurrences of manganese nodules are known from the Clarion-Clipperton Zone in the NE equatorial Pacific, the Peru Basin in the SE Pacific, the Cook Island region in the SW Pacific, the central Indian Ocean Basin, and the Baltic Sea.

T. Kuhn (✉) • A. Wegorzewski • C. Rühlemann • A. Vink
Federal Institute for Geosciences and Natural Resources (BGR),
Stilleweg 2, 30655 Hannover, Germany
e-mail: thomas.kuhn@bgr.de

2.1 Introduction

Manganese nodules occur as potato-shaped concretions on the seafloor of abyssal plains in about 4000–6000 m water depth in all major oceans. They form two-dimensional deposits on top or within the first 10 cm of the deep-sea sediments (Fig. 2.1). Nodules of the eastern tropical Pacific and the central Indian Ocean are of special economic interest due to their high enrichment of metals such as Ni, Cu, Co, Mo, Li, REE, and Ga (e.g., Hein and Koschinsky 2013). Manganese nodules are also known from shallow seas such as the Baltic Sea and from freshwater lakes, but these nodules have considerably lower contents of valuable metals (Glasby et al. 1997; Hlawatsch et al. 2002).

Exploration for and scientific research on manganese nodules have been carried out intensely since the 1970s. Based on the results of these early studies, the environmental conditions and fundamental processes required for nodule formation are well known today. Modern analytical methods have given us new insights into the growth layers and crystal structures of nodules up to an atomic level. Such methods include, among others, high-resolution transmission electron microscopy (HRTEM), X-ray absorption spectroscopy (EXAFS, XANES), and laser-ablation ICP-MS. Advanced knowledge of the crystallographic structure of manganese oxides as well as their oxidation states, structural positions, and coordination environment of metals can be attributed to the utilization of these new methods (Takahashi et al. 2007; Bodei et al. 2007; Peacock and Sherman 2007a; Manceau



Fig. 2.1 High abundance of large nodules on the seafloor of the Peru Basin (ca. 4000 m water depth; © BGR)

et al. 2014; Wegorzewski et al. 2015). Such knowledge could be fundamental for the development of state-of-the-art tailored metallurgical processing techniques for manganese nodules. Considerable research has also focused on the influence of microbial activity on the formation of Mn oxides (Ehrlich 2000).

In this book section, a review of the current state of knowledge of manganese nodule composition, formation, and occurrence is provided. Firstly, a general description of the macroscopic and microscopic textures of Mn nodules including a review of the various mineralogical nomenclatures of Mn oxides and a suggestion for a general terminology is given. Then, we discuss the chemical composition of nodules with special regard to the metal and trace metal content in nodules of different genesis. The formation of nodules under differing environmental conditions is also discussed. Finally, a brief overview of the main economically interesting occurrences of nodule fields and their characteristics is provided.

2.2 Classification and Description

2.2.1 General Classification

Polymetallic manganese nodules consist of concentrically banded zones of micro-layers around a nucleus. The latter can be composed of indurated sediments, rock particles, biogenetic fragments, or micro-nodules (von Stackelberg and Beiersdorf 1987). Individual layers are characterized by different chemical and mineralogical compositions that are determined by two different growth processes: *hydrogenetic* and *diagenetic* growth (Halbach et al. 1988). *Hydrogenetic* layers form as a result of element precipitation from oxygen-rich seawater (Koschinsky and Halbach 1995; Koschinsky and Hein 2003) and *diagenetic* layers form as a result of element precipitation from suboxic pore water (low oxygen content of $<5 \mu\text{mol O}_2/\text{l}$; Burns and Burns 1978; Glasby 2006; Bodeř et al. 2007; Hein and Koschinsky 2013; Wegorzewski and Kuhn 2014). Manganese nodules are usually composed of mixtures of both layer types. In contrast, ferromanganese crusts which usually form on the hard rock of seamounts often consist purely of hydrogenetic layers.

2.2.2 Macroscopic and Microscopic Descriptions

Manganese nodules occur as a monodisperse layer on the sediment-covered seafloor (Fig. 2.1). They can have different size, shape, and surface morphologies (Fig. 2.2) and can reach a size of up to 15 cm in diameter. Some extremely large specimens of 21 cm have been found in the Peru Basin (von Stackelberg 1997). Nodules can have a spheroidal, ellipsoidal, elongated, discoidal, platy, cauliflower, irregular, and polynodule shape. Nodules from the Clarion-Clipperton Zone (CCZ) in the equatorial NE Pacific and from the Central Indian Ocean Basin (CIOB) predominantly have a

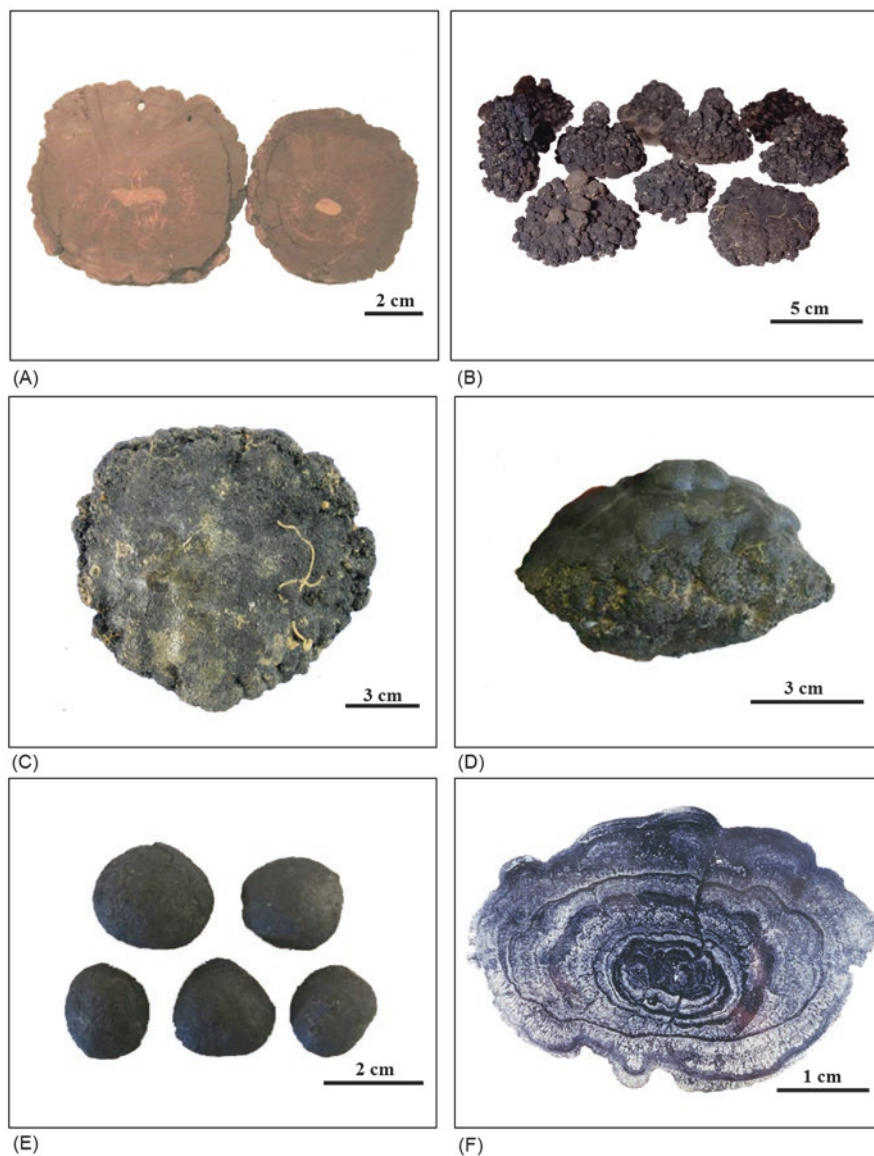


Fig. 2.2 Different sizes and shapes of manganese nodules from different regions. (a) Typical hydrogenetic nodule with a spheroidal shape (from Manihiki Plateau, Cook Islands). (b) Cauliflower-shaped nodules from the Peru Basin. (c) Discoidal-shaped nodule from the Clarion-Clipperton Zone in the equatorial Pacific (CCZ). (d) Nodule with an upper smooth and a lower coarse-grained side. (e) Small, spheroidal nodules from the CCZ. (f) Section through a typical CCZ nodule revealing its layered structure. All figures: © BGR

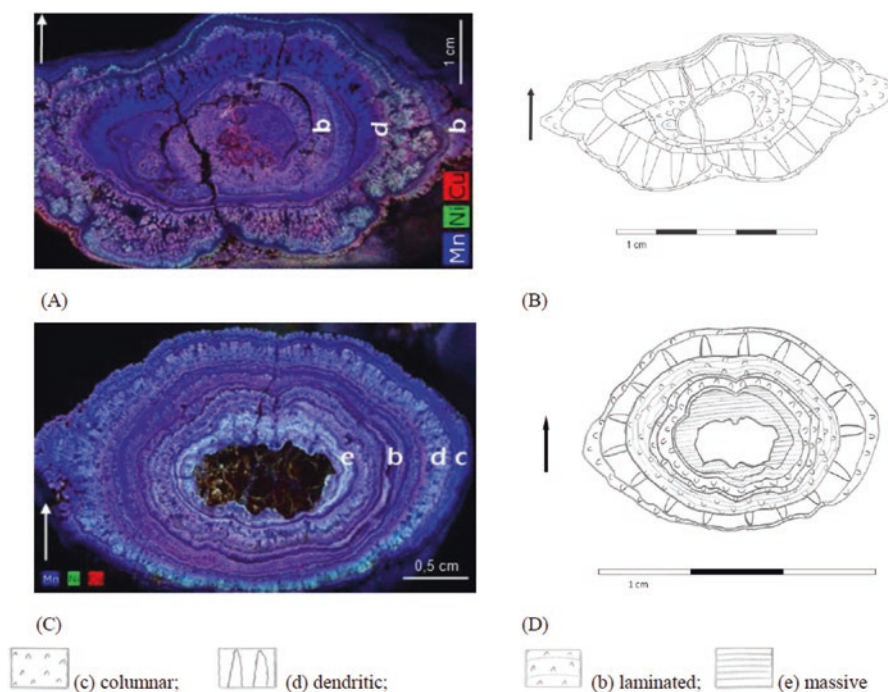


Fig. 2.3 Internal growth structures of manganese nodules. (a, c) Element distribution based on complete scans of the nodule with the Tornado M4 X-ray scanner. (b, d) Internal growth structures based on a combination of X-ray scanner, microscopy, and microprobe analyses. The arrows mark the orientation of the nodule during sampling. See text for further explanation. Figures from Krapf (2014)

discoidal shape and a size range of 2–8 cm. Nodules from the Peru Basin (SE Pacific) are often larger and usually display a cauliflower shape. Hydrogenetic nodules such as those from the Exclusive Economic Zone (EEZ) of the Cook Islands have a predominantly spheroidal shape (Fig. 2.2). Surfaces of nodules are either smooth or coarse-grained, with the smooth side being in contact with seawater and the coarse side being surrounded by sediment.

Depending on the environmental conditions that predominate during nodule formation, hydrogenetic or diagenetic layers with different internal growth structures form (Halbach et al. 1988). These internal growth structures are characterized as being finely laminated, columnar, pillar-like, dendritic, and massive (von Stackelberg and Marchig 1987; Figs. 2.3 and 2.4). Hydrogenetic layers are typically composed of finely laminated to columnar structures, whereas diagenetic precipitation mainly leads to the development of dendritic layers and less frequently to dense, massive layers (Figs. 2.3 and 2.4; Wegorzewski and Kuhn 2014; Krapf 2014). Columnar growth during hydrogenetic precipitation is due to the influence of distinct

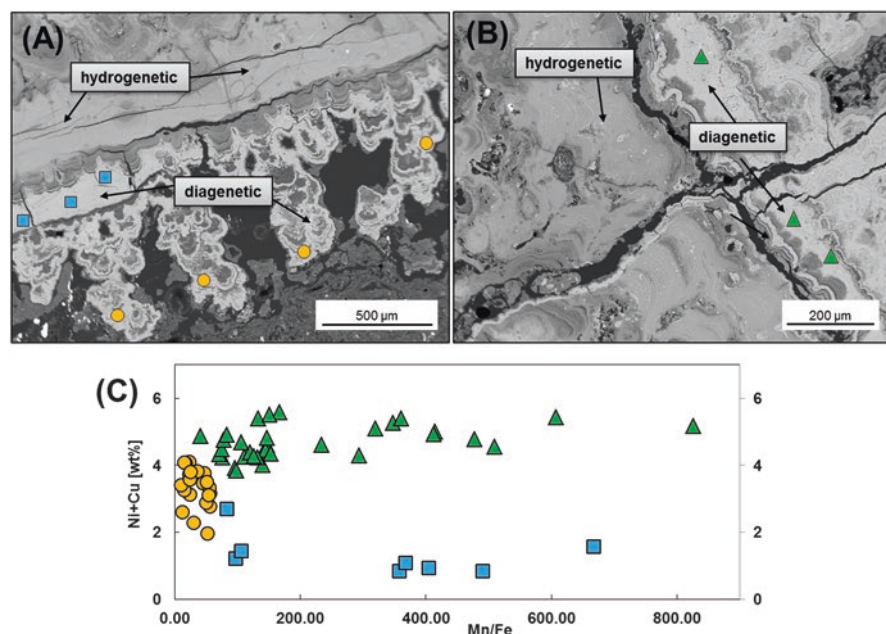


Fig. 2.4 (a, b) Backscatter electron images of typical hydrogenetic and suboxic-diagenetic layers of a manganese nodule from the CCZ. (c) Mn/Fe ratios vs. Ni + Cu contents of individual suboxic-diagenetic layers of the same nodule (Wegorzewski et al. 2015; reproduction with permission of Mineralogical Society of America)

near-bottom currents that not only keep the seafloor sediment-free, but also govern preferential growth on already existing surface areas. In contrast, diagenetic growth takes place within the pore space of the sediments. This often leads to the formation of isolated, rosette-like structures that tend to combine during further growth, thereby encapsulating and incorporating sediment particles.

The growth rate of hydrogenetic layers is typically in the range of 1–5 mm per million years, (Koschinsky and Hein 2003 and references therein, whereas diagenetic layers grow considerably faster (up to 250 mm per million years; von Stackelberg 2000). Altogether, Mn nodules grow with average rates of 10–20 mm per million years and usually have an age of several millions of years.

The dry bulk density of nodules ranges between 1.00 and 2.40 g/cm³, porosity is in the range of 25–61%, and internal surface area lies in the range of 100–150 m²/g (Hein et al. 2013; Blöthe et al. 2015).

The high porosity, the large pore size, and the pore connectivity (high permeability) all enable bottom seawater or pore water to enter the nodules constantly during formation. This is very likely the cause for the secondary fillings of pore spaces with either diagenetic or hydrogenetic precipitates (Wegorzewski and Kuhn 2014; Blöthe et al. 2015).

2.3 Chemical and Mineralogical Composition

2.3.1 Chemical Composition

The chemical composition of nodules is controlled by the type of formation (diagenetic versus hydrogenetic), the location (geographic position and water depth), and the growth rate. Hydrogenetic nodules have Mn/Fe ratios ≤ 5 (Halbach et al. 1988) and high contents of high field strength elements such as Ti, REY, Zr, Nb, Ta, Hf as well as elements that can be oxidized on the surface of Mn oxides such as Co, Ce, and Te (Koschinsky and Hein 2003; Hein et al. 2013). Nodules from the Cook Islands EEZ are mainly of hydrogenetic origin and their element inventory is typical for hydrogenetic nodules (Table 2.1).

Diagenetic nodules are characterized by Mn/Fe ratios > 5 (Halbach et al. 1988) and are enriched with elements that either fit into the crystal lattice of these nodules according to their size or stabilize the lattice by balancing ion charge deficits. The latter is caused either by the incorporation of Mn^{3+} instead of Mn^{4+} into the octahedral chains of Mn oxides, or by vacancy sites therein (see below). Typical elements enriched in diagenetic nodules are Ni, Cu, Ba, Zn, Mo, Li, and Ga. Nodules from the Peru Basin are mainly of diagenetic origin (von Stackelberg 1997) and their element inventory is typical for diagenetic nodules (Table 2.1).

Nodules from the CCZ in the NE Pacific generally exhibit a mixture of diagenetic and hydrogenetic origin, with a predominantly diagenetic input (Wegorzewski and Kuhn 2014; Figs. 2.4 and 2.5). Their elemental contents lie between those typical for hydrogenetic nodules (Cook Islands) and those typical for diagenetic nodules (Peru Basin) with the exception of Cu (1.07% in the CCZ nodules), Ba (3500 $\mu\text{g/g}$), and Mo (590 $\mu\text{g/g}$). The significantly lower Cu content of Peru Basin nodules may be due to a more efficient Cu recycling in carbonate sediments as compared to the siliceous sediments of the CCZ (Wegorzewski and Kuhn 2014). Indian Ocean nodules are also diagenetic–hydrogenetic mixtures, but CIOB nodules generally exhibit lower metal contents as compared to CCZ nodules (Hein et al. 2013).

In addition to the abovementioned abyssal manganese nodules of the large oceans mentioned above, there are many other locations in the world's oceans that host special Mn-(Fe)-nodules. The formation and composition of such nodules are controlled by local conditions such as hydrothermal (seafloor massive sulfides), hydrocarbon (Gulf of Cadiz), and fault-controlled fluid venting (Galicia Bank) or local rapid exchange between oxic and anoxic conditions (Baltic and Black Sea).

Hydrothermal Mn oxides precipitate from low-temperature fluids at the periphery or during the waning stage of a high-T hydrothermal system (Kuhn et al. 2003). Examples are found in almost every seafloor hydrothermal system along mid-ocean ridges, in back-arc basins, and on seamounts. In many cases, they are enriched in manganese (> 40 wt% Mn) and have very low Fe contents (< 1 wt% Fe) and low trace metal concentrations (< 1000 $\mu\text{g/g}$; Table 2.1). However, there can be local exceptions with increased contents of single metals such as the enrichment of molybdenum in some hydrothermal Mn crusts from the SW Pacific (Rogers et al. 2001; Kuhn et al. 2003) or Cu-rich crusts from the Yap island arc (Hein et al. 1992).

Table 2.1 Compiled chemical composition of nodules from selected areas of the global ocean

Element	CCZ ^a		Eastern CCZ ^b		Central CCZ ^b		Peru basin ^a		Indian Ocean ^a		Cook Islands ^c		Gulf of Cadiz ^d		Baltic sea ^e		Fiji basin ^f	
	Mean	N	Mean	N	Mean	N	Mean	N	Mean	N	Mean	N	Mean	N	Mean	N	Mean	N
Fe (%)	6.16	66	6.3	575	6.1	39	6.12	39	7.14	1135	16.1	1158	38.58	36	14.5	0.48	20	
Mn	28.4	66	31.4	575	27.56	39	34.2	39	24.4	1135	16.1	1158	6.03	36	18.1	40.23	20	
Si	6.55	12	6.04	523	7.49	17	4.82	17	10.02	36	7.3	209	3.48	36	–	–	–	
Al	2.36	65	2.29	575	2.71	39	1.5	39	2.92	49	3.01	209	1.38	36	1.02	0.78	20	
Mg	1.89	66	1.94	575	2	39	1.71	39	1.99	53	1.34	204	1.83	36	1.25	1.08	20	
Ca	1.7	66	1.68	575	1.68	39	1.82	39	1.67	53	1.95	209	3.15	36	1.53	1.63	20	
Na	1.99	66	2.19	575	2.04	39	2.65	39	1.86	38	1.84	209	0.26	36	–	–	–	
K	0.99	66	0.97	575	1.09	39	0.81	39	1.14	49	0.89	209	0.34	36	0.86	–	–	
Ti	0.32	66	0.26	566	0.33	39	0.16	39	0.42	53	1.2	74	0.1	36	–	0.04	20	
P	0.21	66	0.15	575	0.21	38	0.15	38	0.17	46	0.34	54	0.19	36	1.48	0.04	20	
Cl	0.27	12	0.7	497	0.46	27	>0.50	27	–	–	0.42	54	–	–	–	–	–	
LOI	26.5	12	15.2	497	15.1	27	16.2	27	–	–	27.7	54	18.05	24	–	–	–	
H ₂ O [–]	11.6	12	–	–	–	–	–	–	–	–	12.7	54	–	–	–	–	–	
H ₂ O ⁺	8.8	7	–	–	–	–	–	–	–	–	11.8	54	–	–	–	–	–	
CO ₂	–	–	–	–	–	–	–	–	–	–	–	–	–	–	–	–	–	
ST	0.17	12	0.16	497	0.1	–	–	–	–	–	–	–	0.12	24	–	–	–	
Ag (ppm)	0.17	12	–	–	–	–	0.05	–	–	–	0.23	49	–	–	–	–	–	
As	67	12	83	497	65	27	65	27	150	3	147	69	159	34	–	–	–	
Au (ppb)	4.5	9	–	–	–	–	–	–	–	–	6	18	<d/l	10	–	–	–	
B (ppm)	–	–	–	–	–	–	–	–	–	–	–	–	278	10	–	–	–	
Ba	3500	66	4304	566	2280	39	3158	39	1708	42	1160	54	352	34	–	390	20	
Be	1.9	12	–	–	1.9	18	1.4	18	–	–	3.9	54	–	–	–	–	–	
Bi	8.8	12	8.4	60	7.25	4	3.3	4	–	–	11	54	<d/l	34	–	–	–	

Br	-	-	-	-	-	-	-	-	-	-	-	-	-	-	-	-	-	-	-
Cd	16	12	-	-	-	-	-	-	-	-	-	-	-	-	-	-	-	-	-
Co	2098	66	1738	575	2501	39	475	1111	1124	4113	1158	90	34	60	11	20	-	-	-
Cr	17	12	14	9	18	4	16	18	3	59	54	34	34	70	-	-	-	-	-
Cs	1.5	61	1.34	566	1.51	18	0.78	0.99	3	<0.38	54	-	-	-	-	-	-	-	-
Cu	10,714	66	11,785	575	10,813	39	5988	10,406	1124	2262	1158	39	34	19.1	47	20	-	-	-
Ga	36	12	25.7	45	-	-	32	-	-	<10	54	-	-	-	-	-	-	-	-
Ge	-	-	-	-	-	-	0.6	-	-	-	-	-	-	-	-	-	-	-	-
Hf	4.7	66	4.53	565	4.51	39	4.7	14	3	13	49	-	-	-	-	-	-	-	-
Hg (ppb)	18	3	-	-	-	-	16	-	-	<36	28	-	-	-	-	-	-	-	-
In (ppm)	0.27	12	-	-	-	-	0.08	-	-	-	-	-	-	-	-	-	-	-	-
Li	131	66	133	566	123	39	311	110	38	51	54	17	10	b.d.	459	20	-	-	-
Mo	590	66	622	567	556	39	547	600	38	295	79	47	34	126	958	20	-	-	-
Nb	22	66	18.7	566	21.3	39	13	98	3	90	67	5	34	-	-	-	-	-	-
Ni	13,002	66	14,012	575	13,574	39	13,008	11,010	1124	3805	1145	108	34	67	115	20	-	-	-
Pb	338	66	276	566	358	39	121	731	38	897	202	18	34	-	<10	20	-	-	-
Rb	23	66	20.2	566	25.2	39	12	70	3	15	54	17	34	-	-	-	-	-	-
Sb	41	12	75	90	19	5	61	50	3	36	54	-	-	-	-	-	-	-	-
Sc	11	66	10.1	566	12	39	7.6	25	3	12	54	18	34	-	-	-	-	-	-
Se	0.72	12	-	-	-	-	0.5	-	-	<0.80	54	-	-	-	-	-	-	-	-
Sn	5.3	12	-	-	-	-	0.9	-	-	7.8	54	-	-	-	-	-	-	-	-
Sr	645	66	701	575	592	39	687	709	53	935	54	282	34	-	380	20	-	-	-
Ta	0.33	66	0.27	559	0.33	39	0.23	1.8	3	2.2	54	-	-	-	-	-	-	-	-
Te	3.6	66	3.57	528	3.85	23	1.7	40	3	24	54	-	-	-	-	-	-	-	-
Tl	199	12	-	-	-	-	129	347	3	146	54	-	-	-	-	-	-	-	-
Th	15	66	11.5	566	17.7	39	6.9	76	3	37	67	4	34	-	-	-	-	-	-
U	4.2	66	3.78	566	3.79	39	4.4	16	3	10	67	4	34	-	-	-	-	-	-
V	445	66	617	575	486	39	431	497	16	508	61	339	34	-	88	20	-	-	-

(continued)

Table 2.1 (continued)

Element	CCZ ^a		Eastern CCZ ^b		Central CCZ ^b		Peru basin ^a		Indian Ocean ^a		Cook Islands ^c		Gulf of Cadiz ^d		Baltic sea ^e		Fiji basin ^f	
	Mean	N	Mean	N	Mean	N	Mean	N	Mean	N	Mean	N	Mean	N	Mean	N	Mean	N
W	62	66	64.3	566	55	39	75	39	92	3	64	67	—	—	—	—	—	—
Y	96	66	78.9	566	105	39	69	39	108	38	141	54	—	—	—	—	—	—
Zn	1366	66	1544	566	1228	39	1845	39	1207	692	545	222	62	34	616	158	20	20
Zr	307	66	302	566	287	39	325	39	752	3	524	75	63	34	—	—	—	—
La	114	66	101	566	109	39	68	39	129	50	173	54	—	—	—	—	—	—
Ce	284	66	242	566	270	39	110	39	486	24	991	54	—	—	—	—	—	—
Pr	33.4	66	29.7	566	33.3	39	14.1	39	33	37	40.9	54	—	—	—	—	—	—
Nd	140	66	120	566	137	39	63	39	146	50	160	54	—	—	—	—	—	—
Sm	34	66	29.8	566	33.9	39	14	39	32.4	50	34.7	54	—	—	—	—	—	—
Eu	8.03	66	7.3	566	8.26	39	3.87	39	7.83	46	8.53	54	—	—	—	—	—	—
Gd	31.8	66	29.3	566	32.6	39	15.6	39	32	24	36.1	54	—	—	—	—	—	—
Tb	4.98	66	4.45	566	5.05	39	2.52	39	5	37	6.09	54	—	—	—	—	—	—
Dy	28.5	66	25.7	566	29.2	39	15.8	39	26.5	46	34.9	54	—	—	—	—	—	—
Ho	5.35	66	4.69	566	5.37	39	3.42	39	4.92	46	7.18	54	—	—	—	—	—	—
Er	14.6	66	13	566	14.9	39	9.8	39	12.9	24	19.1	54	—	—	—	—	—	—
Tm	2.11	66	1.79	566	2.05	39	1.49	39	2	11	3.02	54	—	—	—	—	—	—
Yb	13.7	66	12.5	566	13.7	39	10.3	39	11.8	46	19.8	54	—	—	—	—	—	—
Lu	2.05	66	1.84	566	2.03	39	1.61	39	1.93	50	2.98	54	—	—	—	—	—	—
Ir (ppb)	2	11	—	—	—	—	—	—	—	—	5	19	—	—	—	—	—	—
Os	—	—	—	—	—	—	—	—	—	—	2	11	—	—	—	—	—	—
Pd	8	12	—	—	—	—	—	—	—	—	7	19	—	—	—	—	—	—
Pt	128	12	0.11	7	—	—	40	—	—	—	210	32	—	—	—	—	—	—
Rh	9	12	—	—	—	—	—	—	—	—	17	19	—	—	—	—	—	—
Ru	12	12	—	—	—	—	—	—	26	—	18	19	—	—	—	—	—	—

ΣREY (ppm)	813		701		801	–	403	1039	–	1678	54	78	24	–	–	–
ΣHREY	199	–	172		655	210	130	205	–	–	–	10	24	–	–	–
Element ratios																
Mn/Fe	4.61	66	5.15	575	4.52	39	5.59	3.42	1135	1.00	1158	0.16	36	1.23	83.81	20
Co + Cu + Ni (%)	2.58	66	2.75	575	2.69	39	19.471	22.527	1124	3461		237	36	146.1	173	20
Y/Ho	17.94	66	16.9	566	19.54	39	18.13	21.95	38	–	–	–	–	–	–	–
Zr/Hf	65.32	66	67.2	566	63.64	39	69.15	53.71	3	–	–	–	–	–	–	–
Th/U	3.57	66	3.04	566	4.67	39	1.57	4.75	3	3.7	67	1	24	–	–	–
Ce/Ce	–	–	–	–	–	–	–	–	–	–	–	–	–	–	–	–

Units of elements: Fe-ST: %, rest ppm if not otherwise stated

^aHein et al. (2013)

^bBGR data

^cHein et al. (2015)

^dGonzález et al. (2012)

^eHlawatsch et al. (2002)

^fRogers et al. (2001)

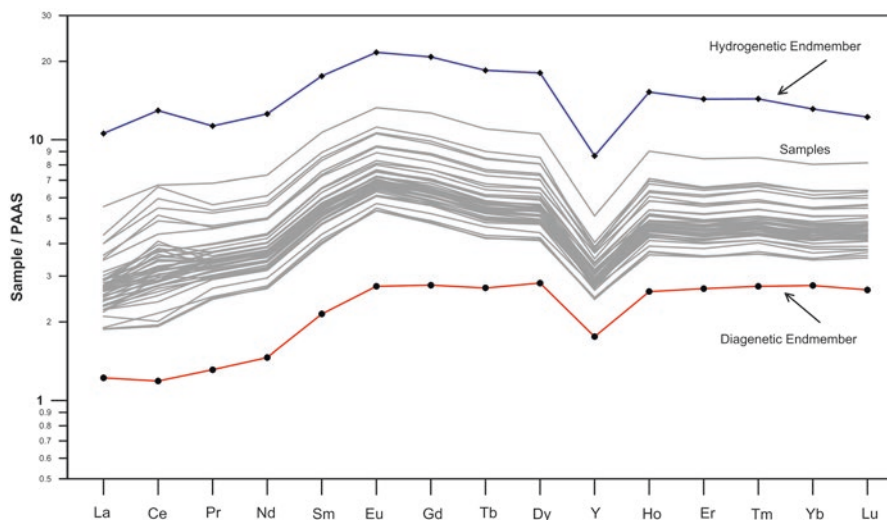


Fig. 2.5 Shale (PAAS) normalized rare earth element and yttrium contents (REY) of manganese nodules from the eastern CCZ (N=47) indicate that the nodules are mixtures of diagenetic and hydrogenetic endmembers (unpublished BGR data; measured with ICP-MS). Diagenetic endmember: nodule from Peru Basin. Hydrogenetic endmember: Fe-Mn crust from CCZ (unpublished BGR data). PAAS Post-Archean Australian Shale (McLennan 1989)

Hydrothermal Mn oxide precipitates form by rapid precipitation from low-T hydrothermal fluids at the contact with cold, oxidizing seawater.

Hydrocarbon-related ferromanganese nodule fields occur in the Gulf of Cadiz in 850–1000 m water depth. Their formation is related to hydrocarbon seeps, mud diapirism, and the activity of strong near-bottom currents (González et al. 2012). The nodules grow rapidly (102–124 mm/Ma) and are characterized by a high Fe-Mn fractionation (39 wt% Fe, 6 wt% Mn) and low contents of trace metals (probably due to the high growth rates; Table 2.1).

Cobalt-rich manganese nodules occur together with extensive phosphorite pavements on seamounts and banks on the western Galicia continental margin (NE Atlantic) in ~1200–2000 m water depth (González et al. 2014). These oxidic precipitates are exceptional since they are not only very rich in Co (up to 1.8%) and Mn (up to 45%), but also contain other trace metals such as Ni, Ti, Cu, Mo, REE, Tl, Ga, and Te in high concentrations (González et al. 2014). The formation of these nodules and phosphorites is at least partly related to the activity of deep-reaching faults and the mobilization of metals from a deeper crustal reservoir (J. González, pers. comm.).

In the Baltic Sea, the abundant occurrence of ferromanganese nodules and concretions (up to 40 kg/m²) is related to the large input of Mn- and Fe-rich suspended matter through rivers in the northeast and east (Gulf of Bothnia, Gulf of Finland) and the formation of an oxidized layer in the upper 2–15 cm of the sediment column (Glasby et al. 1997). Fast-growing Fe-Mn concretions are mainly found in the western Baltic Sea, their formation being related to the development of summer anoxia and the diagenetic mobilization of Mn. The trace metal content of Baltic Sea ferro-

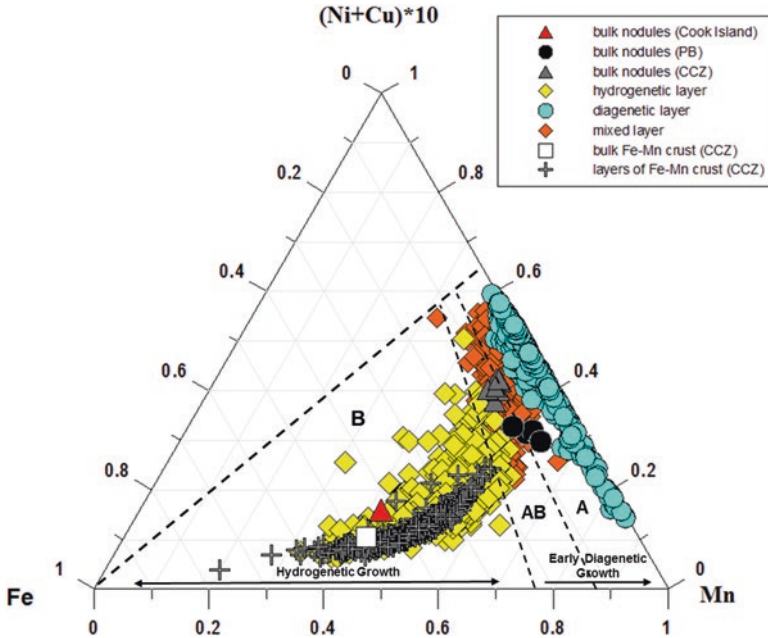


Fig. 2.6 Ternary diagram of Fe-Mn-(Ni + Cu)*10 according to Bonatti et al. (1972) and Halbach et al. (1988) showing the geochemical relationship between different genetic types of nodules and their individual growth layers. Dashed lines separate three nodule-type fields: A diagenetic nodules, AB mixed-type nodules, and B hydrogenetic nodules. Bulk analysis of a ferromanganese crust sample lies in field B (hydrogenetic growth) but the individual analyses of the crust profile show a high variability in the chemical composition. Analyses of individual hydrogenetic layers within the nodules partly show a diagenetic influence (AB). Mixed layers plot into field AB and suboxic-diagenetic layers completely into field A (suboxic-diagenetic). Bulk nodules from both the CCZ and the PB plot into the mixed-type field (AB). Individual layers of nodules, however, show very high scatter as well as much higher Mn/Fe and Ni+Cu concentrations than the bulk nodules. The average bulk nodules from the Cook Islands EEZ show typical hydrogenetic growth and plot into field B (data from Hein et al. 2015). Figure from Węgorzewski and Kuhn (2014). Reproduction with permission of Elsevier

manganese oxides is generally low (<0.1%) compared to the nodules from the open oceans (Table 2.1).

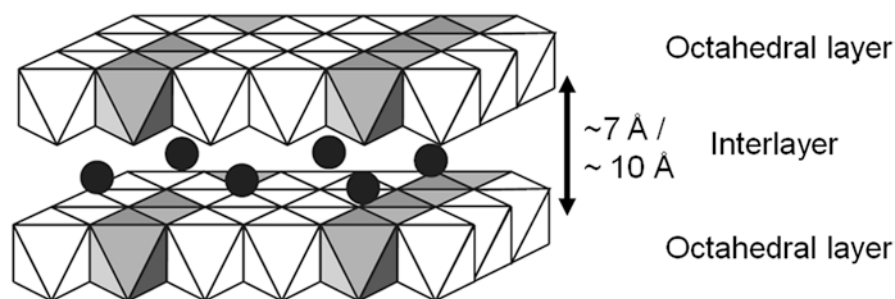
Conventionally, a ternary Mn–Fe–Cu+Ni diagram is used to distinguish between the different modes of formation of manganese nodules and ferromanganese crusts (Bonatti et al. 1972; Halbach et al. 1988). In Fig. 2.6, data from seven bulk manganese nodules and one ferromanganese crust from the CCZ and five bulk nodules from the Peru Basin are displayed together with numerous single layer measurements of the same crust and nodules deriving from electron microprobe analyses (EMP; size of measuring points: 1–20 μm ; Węgorzewski and Kuhn 2014). It is clear that the single layers of the nodules have a much wider spread within this ternary diagram than the respective bulk nodules (Fig. 2.6), indicating that the bulk nodule content only represents the average concentration of all the single layers (Węgorzewski and Kuhn 2014). Therefore, the chemical composition of bulk nodules must be interpreted with care when inferring the genesis of the nodules.

2.3.2 Mineralogical Composition

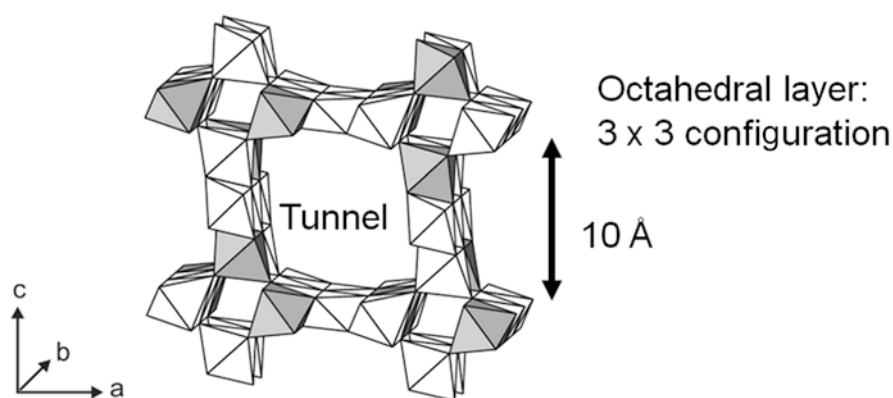
As there is no clear terminology with respect to the usage of mineralogical names of Mn oxides at present, we will try to provide a systematic description of their crystallographic structure and suggest a practical terminology in this chapter.

Manganese nodules consist of different Mn oxides and Fe oxyhydroxides. With respect to the Mn oxides, there are two different groups of minerals occurring in natural manganese nodules: phyllomanganates and tectomanganates. They are both built up of $[\text{MnO}_6]$ octahedral layers which are separated from each other either by an interlayer containing hydrated cations (phyllomanganates) or they are organized in the form of three-dimensional tunnel structures (tectomanganates, Fig. 2.7; Chukhrov et al. 1979; Turner and Buseck 1979; Bodeř et al. 2007). Phyllomanganates can be subdivided into an ordered (birnessite-buserite) and a disordered group (vernadite). Ordered phyllomanganates with a layer-to-layer distance of $\sim 7\text{\AA}$ are named birnessite and contain one plane of water molecules within the interlayer. Ordered phyllomanganates with a layer-to-layer distance of $\sim 10\text{\AA}$ are named buserite and contain two planes of water in the interlayer space (Giovanoli et al. 1975; Burns and Burns 1977; Golden et al. 1986; Post and Veblen 1990; Drits et al. 1997; Bodeř et al. 2007; Węgorzewski et al. 2015). The disordered equivalents to these ordered phyllomanganates are termed 7\AA vernadite and 10\AA vernadite (Manceau et al. 1992a, 2014; Usui and Mita 1995; Drits et al. 1997; Villalobos et al. 2003; Węgorzewski et al. 2015). The crystallographic disorder is termed turbostratic (Warren 1941) because of the random rotation of the $[\text{MnO}_6]$ octahedral layers around the c^* axis or the translation of the $[\text{MnO}_6]$ octahedral layers in the a – b plane of the crystallites (Fig. 2.7; Giovanoli 1980; Drits and Tchoubar 1990). Ordered and disordered phyllomanganates can be distinguished by different peaks (reflections) in their diffraction patterns (Fig. 2.8; Drits et al. 2007).

The $[\text{MnO}_6]$ octahedral layers of phyllomanganates can contain abundant isomorphic substitution of Mn^{4+} (for example by Mn^{3+} , Ni^{2+} , Cu^{2+} , Co^{3+}) but they can also contain vacancies, i.e., empty octahedrons (cf. Fig. 2.7). In either case, layer charge deficits are induced which can be balanced by incorporation of hydrated interlayer cations either into the middle of the interlayer (e.g., Na^+ , Li^+ , Ca^{2+}) or directly above/below layer vacancies (e.g., Mn^{2+} , Mn^{3+} , Ni^{2+} , Cu^{2+} , Zn^{2+} , Cr^{2+} ; Post and Bish 1988; Manceau et al. 1997, 2014; Lanson et al. 2000; Peacock and Sherman 2007a, b). Todorokite consists of edge-sharing, 3×3 $[\text{MnO}_6]$ octahedral chains forming a 3D tunnel structure (Fig. 2.7; Chukhrov et al. 1979; Post et al. 2003; Bodeř et al. 2007). The negative layer charge of todorokite originates from substitution of Mn^{4+} by cations of lower valance (e.g., Mn^{3+} , Ni^{2+}) in the octahedrons. It is balanced by incorporation of mono- and divalent cations into the tunnel structure (e.g., Mg^{2+} , Ba^{2+} ; Fig. 2.7). In general, phyllomanganates have a higher layer charge and accordingly a higher potential to sorb metals (e.g., Ni up to 5%) than todorokite ($\text{Ni} \leq 2\%$; Bodeř et al. 2007).



Phyllosilicates: Birnessite / Buserite



Tectomanganates: Todorokite

Fig. 2.7 Schematic drawings of the spatial organization of octahedral sheets in different types of manganates. Manganates are built up of $[\text{MnO}_6]$ octahedrons (a central Mn^{4+} ion surrounded by 6 oxygen ions in octahedral coordination) which form octahedral layers. In phyllosilicates, these octahedrons form sheets which are stacked in the crystallographic c direction. In tectomanganates, the octahedral sheets form 3D structures such as tunnels. The octahedral sheets contain vacancy sites or $\text{Mn}^{2+}/\text{Mn}^{3+}$ instead of Mn^{4+} , causing a negative charge deficit. The latter is balanced by cations such as Ni^{2+} and Cu^{2+} (black dots) that are located either in the interlayer or the tunnel, or replace Mn ions in the octahedral layer (after Manceau et al. 2012; reproduction with permission of Mineralogical Society of America)

The mineralogical analysis of mainly diagenetic surface nodules from the CCZ and the Peru Basin indicates that nodules from both regions consist of disordered phyllosilicates; todorokite only occurs in minor amounts, if at all (Fig. 2.9; Węgorzewski et al. 2015). This result supports the findings of Usui et al. (1989) and Bodei et al. (2007) who proposed that marine Mn oxides may consist of two series of manganates: a hydrothermal todorokite-like series and a diagenetic buserite-like series.

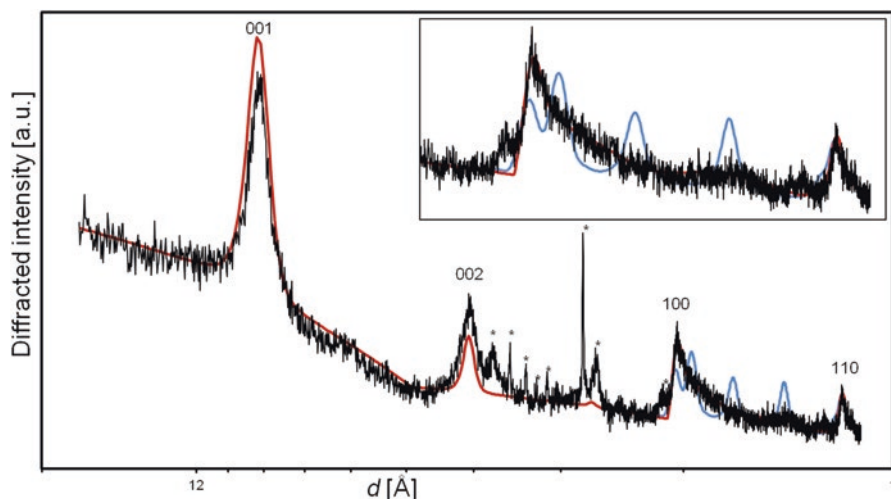


Fig. 2.8 X-ray diffraction pattern of a typical CCZ nodule (*black solid line*) and calculated patterns of a turbostratic (disordered) vernadite (*red line*) and an ordered birnessite (*blue line*). The vernadite and birnessite patterns can be distinguished based on the high angle region (*insert*). The diffractogram of the nodule is similar to the vernadite pattern (*red line*) and different from the birnessite (*blue line*). Several nodules from the CCZ and Peru Basin show similar diffraction patterns, indicating the dominance of disordered phyllomanganates (from Wegorzewski et al. 2015; reproduction with permission of Mineralogical Society of America)

Phyllomanganates can take up many different cations such as alkali, alkali-earth, and transition metals in different amounts and ratios. However, the amount of base metal (Ni, Cu) incorporated into phyllomanganates (Fig. 2.4) does not appear to be dependent on the crystal structure or on the Mn content of the mineral phase, but rather appears to be controlled by the different availability of the respective metal due to varying environmental conditions (Wegorzewski et al. 2015). For instance, nodules from the CCZ and the Peru Basin are composed of the same turbostratic phyllomanganates, yet they have different Cu contents (0.6% versus 1.1%, see above). By taking up the available metals and other cations, the phyllomanganate crystal structure is stabilized or probably can form at all. After formation, different post-depositional exchange processes may lead to the release or uptake of metals and eventually to the stabilization of the phyllomanganate structure. Such post-depositional alteration processes can even lead to the formation of todorokite from a phyllomanganate precursor (Bodei et al. 2007).

In contrast to abyssal diagenetic manganese nodules, hydrothermal Mn oxides mainly consist of well-crystallized todorokite (Kuhn et al. 2003 and references therein). This is probably due to the higher levels of energy available in a hydrothermal system and the relatively fast growth rates of hydrothermal precipitates. Table 2.2 provides an overview of the mineralogical phases and the crystal characteristics that characterize marine manganese oxide precipitates.

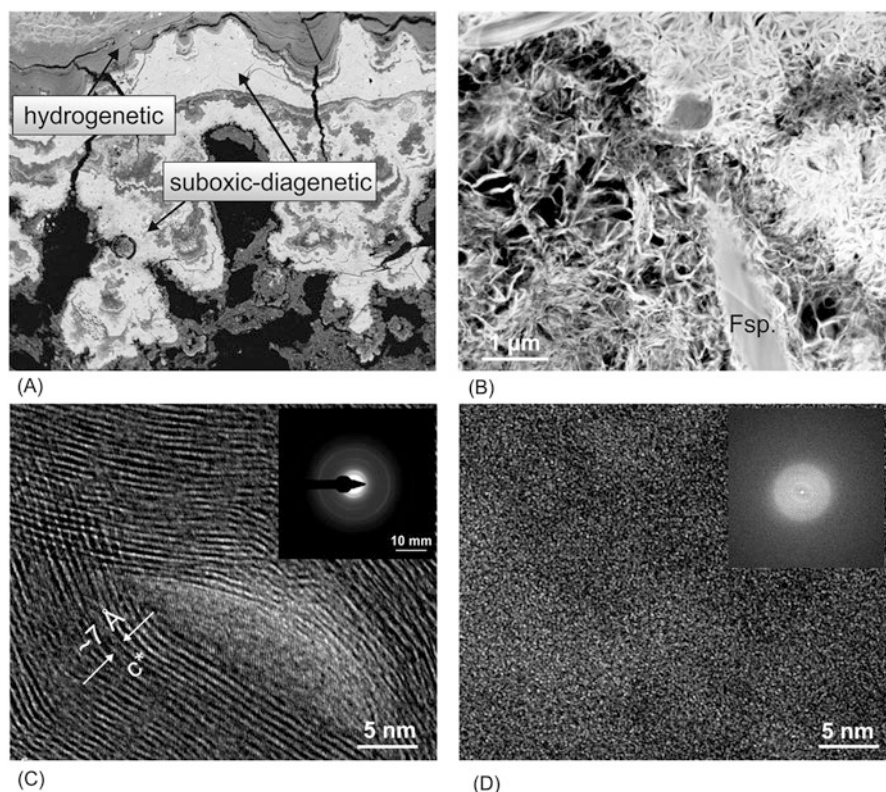


Fig. 2.9 (a) Backscatter electron image of two different types of growth layers of a manganese nodule. (b) High-resolution image (high-angle annular dark field) of dendritic-diagenetic growth structures (for location, see *rectangle* in a). (c) HRTEM image of a diagenetic layer (*insert*: corresponding electron diffraction pattern) indicating reflections typical for 10 Å and 7 Å phyllomanganates. (d) HRTEM image of a hydrogenetic layer (*insert*: corresponding SAED pattern) without any lattice fringes or reflections (figures from Węgorzewski et al. 2015; reproduction with permission of Mineralogical Society of America)

2.4 Formation of Manganese Nodules

There are three principal processes leading to the formation of ferromanganese oxides under marine conditions: hydrogenetic precipitation, diagenetic precipitation, and precipitation from hydrothermal fluids.

2.4.1 Hydrogenetic Precipitation

The formation of Mn and Fe oxide colloids in oxic seawater and their precipitation onto hard ground is called hydrogenetic precipitation (Halbach et al. 1988; Koschinsky and Halbach 1995; Koschinsky and Hein 2003 and references therein).

Table 2.2 Characterization of the main different Mn oxide minerals that can occur in manganese nodules

	Mineral name	Basal reflections		Stacking mode	Layer symmetry	Diagnostic reflections (00l reflections omitted)	Note
		[001] [002]	Ability to collapse				
Vernadite ^a group/ δ - MnO ₂ ^b	7 Å vernadite ^c	~7 Å; ~3.5 Å	Yes	Turbostratic	Hexagonal	hk bands: 2.40–2.45 and 1.41–1.42 Å	Nanocrystals, the band at ~2.4 Å is asymmetric, one water layer in-between two Mn-O-octahedral sheets, vacancies occur within the Mn-O-octahedral sheets, typical interlayer cation: e.g., K ⁺
					Orthogonal	hk bands: ~2.4 and ~1.52, 1.4 Å	Nanocrystals, ~2.4 Å band is asymmetrical, the band at ~1.4 Å is split in two, one water layer between two Mn-O-octahedral sheets, Mn ³⁺ cations are arranged in rows parallel to the <i>b</i> axis, one row of Mn ³⁺ cations is followed by two rows of Mn ⁴⁺ , interlayer cation: e.g., K ⁺
	10 Å vernadite ^c	~10 Å; ~5 Å	Depending on the triple corner (TC) species over layer vacancies, which can stabilize the structure against collapsing	Turbostratic	Hexagonal	hk bands: 2.40–2.45 and 1.41–1.42 Å	Nanocrystals, ~2.4 Å band is asymmetrical, two water layers between two Mn-O-octahedral sheets, vacancies occur within the Mn-O-octahedral sheets, typical interlayer cation: e.g., Mg ²⁺
					Orthogonal	hk bands: ~2.4 and ~1.52, 1.4 Å	Nanocrystals, ~2.4 Å band is asymmetrical, the band at ~1.4 Å is split in two, two water layers within two Mn-O-octahedral sheets, Mn ³⁺ cations are arranged in rows parallel to the <i>b</i> axis, one row of Mn ³⁺ cations is followed by two rows of Mn ⁴⁺ , typical interlayer cation: e.g., Mg ²⁺
	Fe– vernadite ^{c,d}	–	Absent	Turbostratic	Hexagonal	hk bands: 2.40–2.45 and 1.41–1.42 Å	Typically single layers (no basal nor <i>hkl</i> reflections), vernadite is epitaxially intergrown with amorphous δ -FeOOH

Bimessite group	7 Å bimessite ^{e,f}	~7 Å; ~3.5 Å	Yes	Ordered	Hexagonal	hkl are variable, depending on the layer stacking	Ordered three-dimensionally, one water layer in-between two Mn-O-octahedral sheets, vacancies occur within the Mn-O-octahedral sheets, typical interlayer cation: e.g., K ⁺
			Yes	Ordered	Orthogonal	hkl are variable, depending on the layer stacking	Ordered three-dimensionally, one water layer, Mn ³⁺ cations arranged in rows parallel to the <i>b</i> axis, one row of Mn ³⁺ cations is followed by two rows of Mn ⁴⁺ , interlayer cation: e.g., K ⁺
	10 Å busenite ^{g,h,i}	~10 Å; ~5 Å	Depending on the TC species, which can inhibit collapsing	Ordered	Hexagonal	hkl are variable, depending on the layer stacking	Ordered three-dimensionally hydrated form of busenite, two water layers between two Mn-O-octahedral sheets, vacancies occur within the Mn-O-octahedral sheets, typical interlayer cation: e.g., Mg ²⁺
					Orthogonal	hkl are variable, depending on the layer stacking	Ordered three-dimensionally hydrated form of busenite: two water layers between two Mn-O-octahedral sheets, Mn ³⁺ and Mn ⁴⁺ in the octahedral sheets, no significant amounts of vacancies are expected, but the structure has not been refined yet, typical interlayer cation: e.g., Mg ²⁺
	Asbolane ^{j,k}	~10 Å; ~5 Å	Yes	Turbostratic	Hexagonal	Two incommensurate hexagonal networks of hk bands at positions comparable to vernadite, split of the (100) and (110) reflections	Ni(OH) ₂ , Cu(OH) ₂ , Co(OH) ₂ , Co(OH) ₃ or CoOOH between interlayer of two Mn-O octahedral sheets

(continued)

Table 2.2 (continued)

	Mineral name	Basal reflections		Stacking mode	Layer symmetry	Diagnostic reflections (00l reflections omitted)	Note
		[001][002] reflections	Ability to collapse				
	Chalcophanite ^d	~6.9 Å; ~3.5 Å	Yes	Ordered	Hexagonal	hkl: 4.07; 3.51; 2.23; 1.59	One out of seven Mn ⁴⁺ is missing and two Zn ²⁺ O ₆ octahedra are below and above vacancies (one on each side)
	Lithiophorite ^m	~9.4 Å; ~4.7 Å	Unknown	Ordered	Hexagonal	hkl: 2.38; 1.88; 1.58; 1.46; 1.39	Alternately stacked layers of Mn-O and (Al, Li)-OH octahedra
	Todorokite ^{h,k}	No basal reflections but peaks at ~10 Å and ~5 Å (9.7 Å; 4.8 Å)	No (tunnel structure)	Ordered	Layer symmetry is not applicable	hkl: 2.40 (intense and symmetric) and further reflections between 2.2 and 1.7 Å	Tunnel structure with [3 × 3] tunnel size, defective form of todorokite with [3 × n] (n ≤ 9)

^aNatural mineral^bSynthetic form of vernadite^cBoder et al. (2007)^dBurns et al. (1975)^eDrits et al. (1997)^fDrits et al. (2007)^gGiovanoli (1980)^hBurns et al. (1983)ⁱNovikov and Bogdanova (2007)^jManceau et al. (1992)^kManceau et al. (2014)^lPost and Appleman (1988)^mPost and Appleman (1994)

Under normal Eh–pH conditions of seawater ($E_h > 0.5$ V; pH ~ 8), manganese tends to oxidize to $Mn^{4+}O_2$ and iron to $Fe^{3+}OOH$. Both phases are not dissolvable under seawater conditions and form colloids. Moreover, both phases tend to hydrolyze and the hydrolyzed, oxidic surface of these oxides contains OH groups with amphoteric character causing a pH-dependent surface charge. At the seawater pH of ~ 8 , MnO_2 has a strong negative surface charge and δ - $FeOOH$ has a slightly positive surface charge. Thus, the negatively charged MnO_2 colloid particles adsorb dissolved cations such as Co^{2+} , Ni^{2+} , Zn^{2+} , Tl^+ and the slightly positively charged $FeOOH$ particles adsorb all ions that form anionic complexes such as carbonate ($REE(CO_3)_2^-$), hydroxide ($Hf(OH)_5^-$) and/or oxyanion (MoO_4^{2-}) complexes (Koschinsky and Halbach 1995; Koschinsky and Hein 2003; Hein et al. 2013). The enrichment of elements to the Mn oxide surface is the result of strong physical sorption, whereas the enrichment at the $FeOOH$ surface is controlled by chemical bonding such as covalent and coordinative bonds. Both types of colloids eventually combine and precipitate onto sediment-free substrate forming typically hydrogenetic ferromanganese crusts with Mn/Fe ratios around unity. Due to the high internal surface area of hydrogenetic ferromanganese oxides (up to >300 m²/g; Hein et al. 2013), they can enrich elements up to a factor 10^9 over ambient seawater (e.g., Co, Pb, Mn, Ce, Te; Hein et al. 2010).

Elements having more than one oxidation state in the marine environment, and which are dissolved in the lower oxidation state as positively charged cations, can be oxidized at the surface of MnO_2 after adsorption. In this way, certain elements are especially enriched on the surface of ferromanganese oxides. Typical examples for this oxidative scavenging are cobalt (oxidized from Co^{2+} to Co^{3+}), cerium (Ce^{3+} to Ce^{4+}), lead (Pb^{2+} to Pb^{4+}), thallium (Tl^+ to Tl^{3+}), and tellurium (Te^{4+} to Te^{6+}). Surface oxidation may be mediated by coordinated surface OH groups which enable the electron transfer from metal ions to the oxygen molecule (Koschinsky and Hein 2003). Oxidative scavenging on Mn oxide surfaces is inversely correlated to the growth rate of these hydrogenetic phases, as illustrated by a Mn/Fe ratio versus element content diagram (Fig. 2.10). Typical hydrogenetic growth rates range between 1 and 5 mm/million years (Halbach et al. 1988).

Hydrogenetic precipitation leads to the formation of hydrogenetic layers in mixed-type manganese nodules from the CCZ and the Central Indian Ocean Basin and may entirely control the formation of nodules within the EEZ of the Cook Islands (Hein et al. 2015). However, the main products of hydrogenetic precipitation are ferromanganese crusts, as they occur on sediment-free seamount slopes, guyots, and other seafloor areas with outcropping bare rocks. A more detailed discussion of hydrogenetic processes and their products can be found in the chapter on ferromanganese crusts in this book (Halbach et al. this edition).

2.4.2 Diagenetic Precipitation

The formation of Mn nodules due to element precipitation from pore water within the sediment or on the sediment surface is called diagenetic precipitation. This form of Mn oxide precipitation is related to the diagenetic sequence of deep-sea

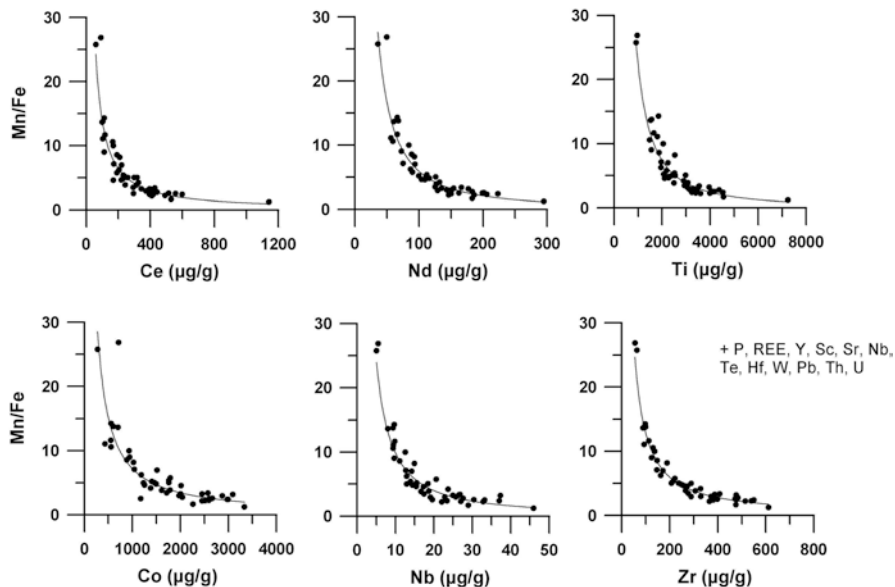
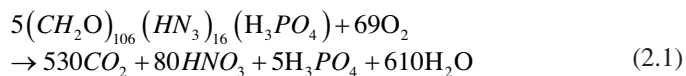


Fig. 2.10 Mn/Fe ratios versus element concentrations of single layers of manganese nodules from the eastern CCZ (BGR data; measured with ICP-OES and -MS). Note the inverse, parabolic curve progression of all elements which is typical for elements enriched by hydrogenetic surface adsorption. The elements listed on the right side exhibit similar geochemical behavior

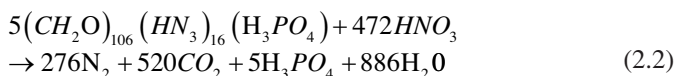
sediments as described in Froelich et al. (1979). The diagenetic sequence is controlled by the oxidation of organic material through a sequence of redox reactions with different electron acceptors. Although the degradation of organic matter is carried out almost exclusively by bacteria, the microorganisms acquire energy for their metabolism through these reactions and the sequence of reactions is controlled by the redox levels and energy yields, starting with redox reactions yielding the highest energy (Stumm and Morgan 1981; Chester and Jickells 2012).

The sequence starts with the reaction of organic material with dissolved oxygen, i.e., aerobic respiration. Aerobic organisms use dissolved oxygen from overlying or interstitial waters to oxidize organic matter according to the following general equation (Galaway and Bender 1982):

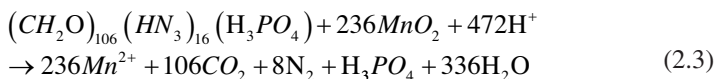


The composition of organic material is represented in this and the following equations by the so-called Redfield composition (Chester and Jickells 2012). The reaction according to (2.1) leads to the formation of nitrate and is also termed “nitrification.” As >90% of the organic material that reaches the seafloor is degraded through its reaction with O_2 , oxygen is regarded as the primary oxidant (Chester and Jickells 2012).

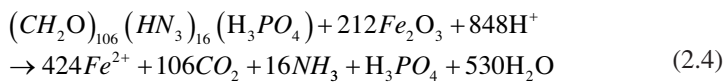
When dissolved oxygen becomes depleted after sufficient consumption, the decomposition of organic matter can continue under anaerobic conditions using secondary oxidants [suboxic diagenesis, (2.2)–(2.4)]. These secondary oxidants are nitrate, MnO_2 , Fe_2O_3 , and sulfate. However, under the conditions typical for the formation of Mn nodules, only nitrate and MnO_2 play a significant role. If the dissolved oxygen level falls to ~5% of the saturation concentration, nitrate becomes the preferred electron acceptor according to the following reaction (“denitrification”):



This denitrification process overlaps with Mn^{4+} as alternative electron acceptor according to:



If Mn^{4+} is consumed, the diagenetic sequence proceeds to Fe^{3+} as electron acceptor according to:



As the different reactions in this diagenetic sequence follow one another consecutively, a respective series of diagenetic zones in the sediments is formed (Fig. 2.11). Organic carbon is oxidized by manganese oxides in zone 4 and dissolved Mn^{2+} is released into interstitial water. This Mn^{2+} then diffuses upwards and is oxidized back to MnO_2 at the top of zone 3 (Chester and Jickells 2012).

The thickness of the respective diagenetic zones in bottom sediments depends on the supply of organic matter, its accumulation rate, and the rate of supply of oxidizing agents (Chester and Jickells 2012). During phases when the top of zone 3 rises close to the sediment–water interface, diagenetic manganese can significantly contribute to the growth of manganese nodules. Processes of manganese and iron reduction do not occur simultaneously in the diagenetic sequence and the environmental conditions that are typical for diagenetic Mn nodule growth occur in zones 3 and 4 (Fig. 2.11). This is the reason for the strong Mn-Fe fractionation within diagenetic layers of manganese nodules (Mn/Fe ratio up to 800; Wegorzewski and Kuhn 2014).

Diagenetic Mn flux rates are considerably higher than hydrogenetic Mn flux rates, which explains the high diagenetic growth rates of up to 250 mm/Myr (von Stackelberg 2000). Thus, the supply of manganese to the position of the manganese nodule is high enough to form crystallized phyllomanganates, in contrast to hydrogenetic precipitates which are composed of cryptocrystalline vernadite (Wegorzewski et al. 2015). However, especially alkali, alkali-earth, and transition metals are required to stabilize the phyllomanganate lattice (see chapter 3.2). Thus,

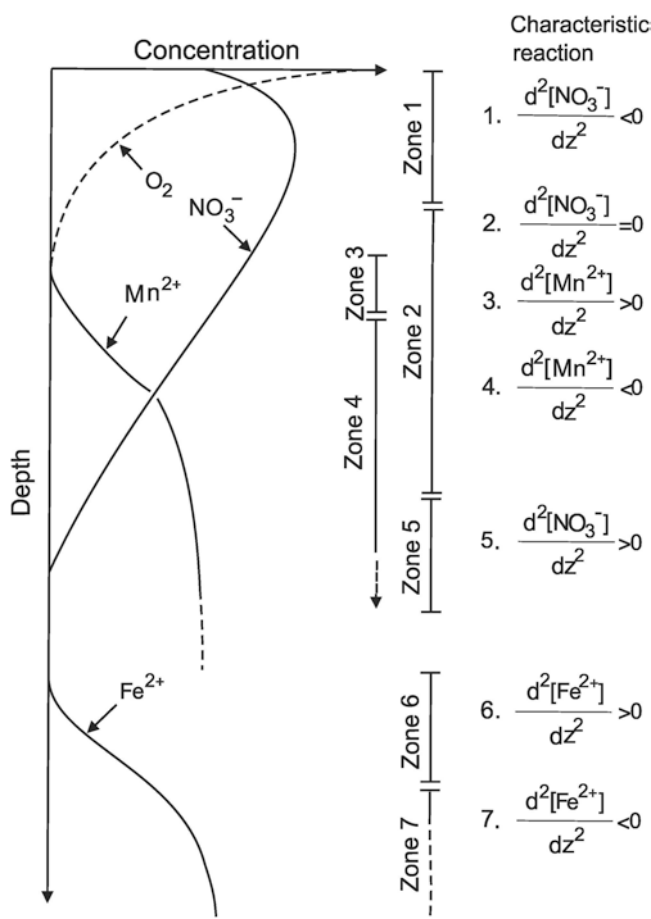


Fig. 2.11 Schematic representation of pore water profiles and different diagenetic zones in deep-sea sediments. In Zone 1 oxygen is the oxidant of organic carbon, in Zones 2–5 nitrate and Mn⁴⁺ are the oxidants and Mn²⁺ is released into pore water. Dissolved Mn²⁺ diffuses upward until it is reoxidized in Zone 3. In Zones 6 and 7 organic carbon is oxidized by ferric iron and Fe²⁺ is released into pore water (from Froelich et al. 1979; reproduction with permission of Elsevier)

metals such as Ni, Cu, Mo, Zn, Ba, and Li are enriched in diagenetic nodules (Fig. 2.12). The general dominance of Ni in diagenetic nodules of the CCZ is probably a result of the relatively high Ni content in the pore water of siliceous deep-sea sediments (Table. 2.3).

Manganese nodules from the Peru Basin are mainly composed of diagenetic layers. The present-day oxic-suboxic front in this area is located at about 10 cm sediment depth and a strong dissolved Mn²⁺ gradient can be observed in the interstitial waters (Koschinsky 2001). In the sediments of the eastern CCZ, the present-day oxic-suboxic front reaches down to a sediment depth of 2–3 m (Mewes et al. 2014) and in the central CCZ the sediment column even appears to be oxic over tens of meters of depth (Müller et al. 1988). The organic carbon content in the surface sediments

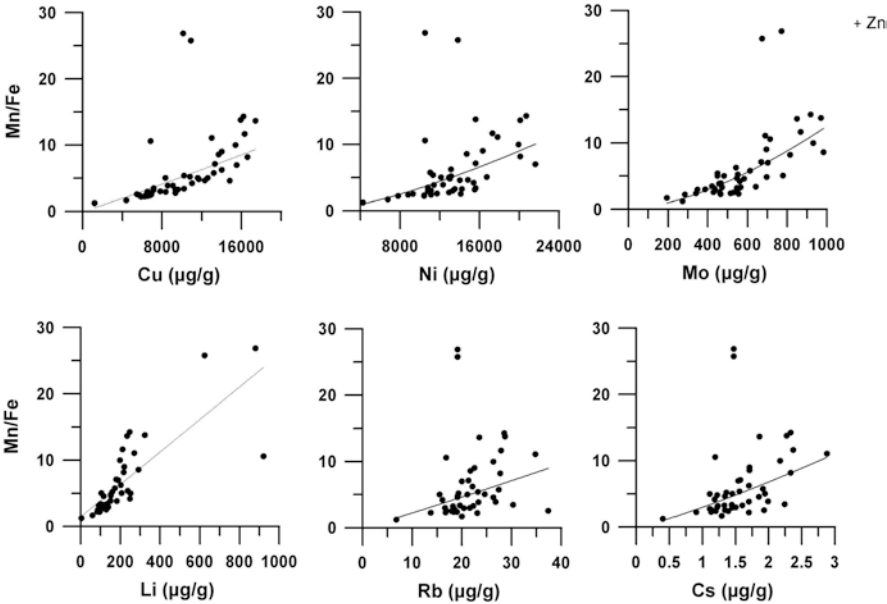


Fig. 2.12 Mn/Fe ratios versus element concentrations of single layers of manganese nodules from the eastern CCZ (BGR data; measured with ICP-OES and -MS). The positive correlation with the Mn/Fe ratio suggests that these elements are incorporated into diagenetic Mn oxides. Note the different curve progression compared to elements enriched by hydrogenetic processes (cf. Fig. 2.10)

Table 2.3 Element contents of interstitial water and seawater of siliceous deep-sea sediments (with up to 14% carbonate content)

	Mn	Fe	Cu	Ni	Co
Oxic pore water ^a	<10	<1	40–80	<50	<5
Suboxic pore water ^a	10,000–100,000	< 1	40–120	200–600	30–60
Near-bottom seawater ^b	0.2–3	0.1–2.5	0.5–6	2–12	0.01–0.1
Principal species in seawater ^c	Mn ²⁺ MnCl ⁺	Fe(OH) ₂ ⁺ Fe(OH) ₃ ⁰ Fe(OH) ₄ ⁻	Cu ²⁺ CuOH ⁺ CuCO ₃ ⁰	Ni ²⁺ NiCl ⁺	Co ²⁺ CoCl ⁺

^aShaw et al. (1990)

^bBruland (1983)

^cByrne (2002). All concentrations in nmol/l

of the Peru Basin is up to >1% (Haeckel et al. 2001), in the eastern CCZ it is between 0.4 and 0.6% (BGR data), and in the central CCZ it is between 0.2 and 0.4% (Müller et al. 1988). Accordingly, Mn nodules from the Peru Basin are thought to be mainly formed by suboxic diagenesis, whereas CCZ nodules apparently have been formed by oxic diagenesis (von Stackelberg 1997; Chester and Jickells 2012). However, Wegorzewski and Kuhn (2014) have shown that the fabric and the chemical composition of the internal growth structures of nodules from both areas are similar, suggesting that the nodules from both areas have been formed by the same genetic processes over time and consist of a mixture of suboxic-diagenetic and oxic-

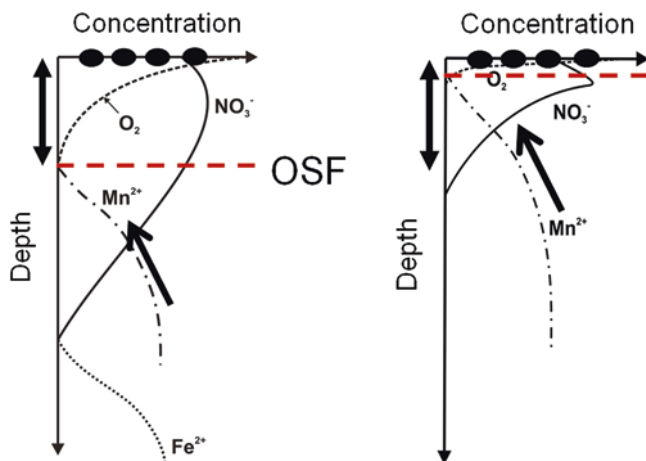


Fig. 2.13 Schematic representation of recent pore water conditions (a) and conditions during former suboxic nodule growth in the eastern CCZ (b). *Black ellipses* represent Mn nodules at the sediment surface. Under recent conditions, there is no suboxic-diagenetic nodule growth. Temporal fluctuations of the OSF (oxic-suboxic front) may be due to variations in the organic carbon flux, e.g., ultimately controlled by climate change. The arrows on the Mn^{2+} profile indicate the direction of the diffusive Mn-flux. If the OSF is close enough to the seafloor, diffusive diagenetic Mn-flux contributes to Mn nodule growth. Under recent oxic conditions (a) Mn nodule growth is only oxic-hydrogenetic (Blöthe et al. 2015). The current OSF reaches down to 2–3 m sediment depth (Mewes et al. 2014)

hydrogenetic layers. Nevertheless, the proportion of hydrogenetic material in CCZ nodules is higher, and hence the metal content of CCZ nodules is in-between that of diagenetic Peru Basin nodules and that of typical hydrogenetic nodules (e.g., from the Cook Islands; Hein et al. 2013, 2015). In order to produce near-surface, suboxic conditions in CCZ sediments (Figs. 2.13 and 2.14) it would be necessary to increase the organic carbon flux to the seafloor by a factor of two, i.e., from a present-day average of $3 \mu\text{mol cm}^{-2} \text{a}^{-1}$ (Mewes et al. 2014) to $\sim 6 \mu\text{mol cm}^{-2} \text{a}^{-1}$, as is the case in the Peru Basin today (Haeckel et al. 2001). Such increases of the organic carbon flux may have occurred during past glacial stages due to enhanced paleoproductivity (Herguera 2000). Moreover, suboxic conditions at the seafloor of the CCZ during glacial stages may also have occurred due to reduced ventilation of the deep ocean as suggested by Bradtmiller et al. (2010).

Irrespective of the absolute oxygen concentrations in bottom and pore waters, oxic diagenesis might only play a minor role in the formation of Mn nodules, as processes of manganese mobilization and transportation in the sediments under oxic conditions are probably limited to the micrometer scale. Diagenetic processes taking place under oxic conditions within the interstitial water seem to be similar to hydrogenetic processes, i.e., enrichment of manganese and other metals is controlled by surface adsorption and oxidation. This assumption is supported by X-ray photoelectron spectroscopy (XPS) measurements of nanometer-thin surface layers of nodules that are in contact with oxic interstitial water (Blöthe et al. 2015). These surface layers have metal contents and elemental ratios that are typical for hydrogenetic precipitation (Wegorzewski and Kuhn 2014).

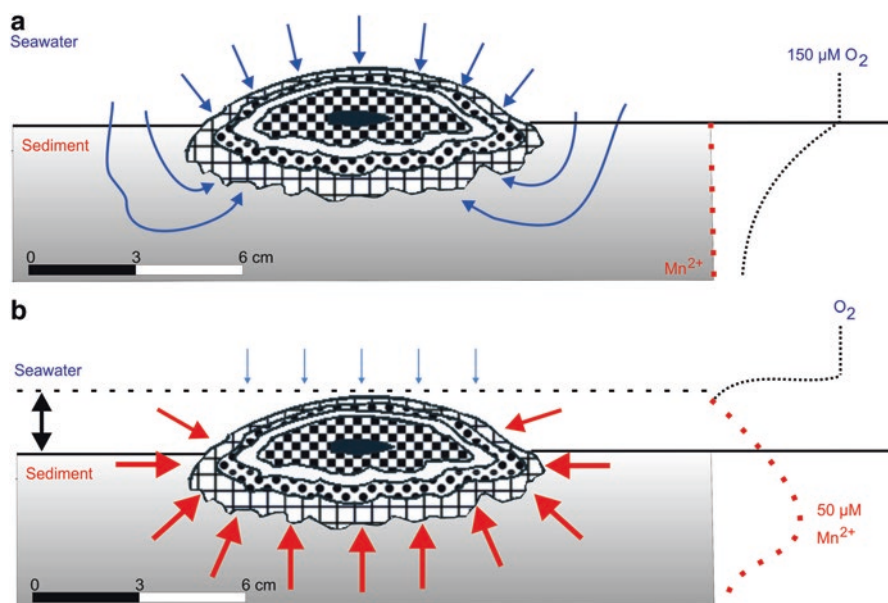


Fig. 2.14 Schematic drawings of recent oxic (a) and fossil suboxic (b) Mn nodule growth in the CCZ. The *black horizontal line* marks the seafloor; *blue arrows* represent hydrogenetic precipitation under oxic conditions, and *red arrows* represent diagenetic precipitation under suboxic conditions. The thickness of the arrows reflects flux rates. The *dotted lines* represent pore water contents of O_2 and Mn^{2+} (data from Mewes et al. 2014). The *black vertical arrow* on the left side (b) indicates that the nodules might have been covered by sediments during suboxic growth phases in order to enable diagenetic layer formation all around the nodules

As mentioned above, manganese nodules occur worldwide throughout the abyssal plains, but special conditions in areas such as the CCZ and the CIOB have yielded economically interesting nodule abundances. Interactions between the position of the carbonate compensation depth, water depth, surface bioproductivity, sedimentation rate, sediment type, benthic activity, near-bottom currents, and local micro-topography determine whether nodule abundances reach values that are high enough to become economically interesting. The CCZ area is located just north of the equatorial high bioproductivity zone (Halbach et al. 1988). The combination of water depth and surface bioproductivity in the CCZ leads to its seafloor being near or just below the carbonate compensation depth (CCD). Areas further to the south (close to the equator) are subject to high bioproductivity and high sedimentation rates, leading to a lowering of the CCD. Under such conditions, widespread manganese nodule growth is hampered (Fig. 2.15). The formation of siliceous ooze close to the CCD provides the necessary metal content and the physical properties (such as permeability for the mobility of metals in pore water) for the growth of large diagenetic nodules. The slow subsidence of the seafloor as well as the slow plate motion to the northwest as a consequence of seafloor spreading and oceanic crust alteration together with a constant sedimentation rate provides optimal conditions over a geological time span (a few million years) for Mn nodule growth. Furthermore, numerous seamounts and fault zones provide a high amount of nucleus

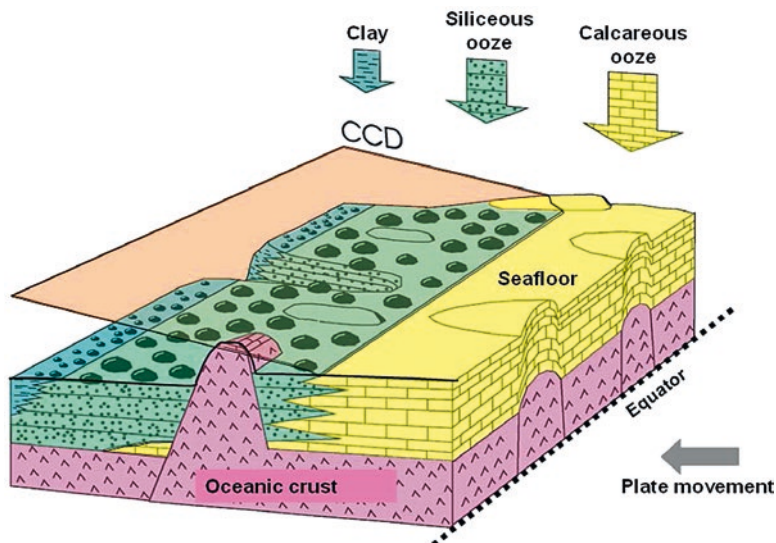


Fig. 2.15 Schematic model of the CCZ area explaining the locations of high and low nodule abundances. Nodules of medium to large size and high abundance occur in areas with medium sedimentation rates at or just below the carbonate compensation depth (CCD) in siliceous ooze. Small-sized nodules of low abundance occur in deep-sea clay with low sedimentation rates and far below the CCD. High bio-productivity at the equator results in high sedimentation rates of predominantly carbonate-rich particles and a deepening of the CCD, thus preventing the formation of manganese nodules. Figure adopted from Beiersdorf (2003); reproduction with permission of International Seabed Authority

material to initiate nodule growth. A flat seafloor over vast areas and moderate near-bottom currents furthermore enable the formation of Mn nodule fields.

Over a period of several million years the CCZ has moved from being an area with optimal conditions for Mn nodule growth to an area with suboptimal conditions, leading to the growth of smaller nodules (Fig. 2.15). This is mainly due to the greater water depths together with lower bioproductivity and particle flux rates, leading to decreasing fluxes of metals and organic material to the seafloor. This leads to a decrease in diagenetic overturn and thus to a smaller diagenetic input to the nodules. These are also the reasons for the lower nodule abundances in the Indian Ocean Basin compared to the CCZ (see above).

2.4.3 Microbial Manganese Mobilization and Deposition

Since several decades, scientists have speculated on the possible influence of microorganisms on the formation of Mn oxides in manganese nodules and ferromanganese crusts. Suggestions have been made that these oxides have not only formed abiotically but that they may form by biologically driven processes due to the activity of microorganisms such as bacteria (Ehrlich 1963; Schweissfurth 1971; Rosson and

Nealson 1982; Villalobos et al. 2003; Webb et al. 2005) and/or fungi (Miyata et al. 2006; Grangeon et al. 2010). Ehrlich (1972) determined three types of bacteria within manganese nodules: Mn^{2+} -oxidizers, Mn^{4+} -reducers, and bacteria which neither oxidize (Mn^{2+}) nor reduce (Mn^{4+}) manganese. A recent study of Blöthe et al. (2015) revealed the occurrence of a diverse prokaryotic community dominated by nodule-specific Mn^{4+} -reducing and Mn^{2+} -oxidizing bacteria (*Shewanella* and *Colwellia*) within manganese nodules from the CCZ. The oxidation of cations scavenged onto the nodules may serve as an energy source for the activity of bacteria living on/in them (Tebo et al. 2004; Ehrlich and Newman 2009).

Several studies were conducted in the laboratory to produce synthetic Mn oxides under the influence of bacteria and fungi (e.g., Bargar et al. 2005; Villalobos et al. 2003; Grangeon et al. 2010). Different products were detected after bacterial Mn(II) oxidation. Hastings and Emerson (1986) as well as Mann et al. (1988) revealed hausmannite (Mn_3O_4), which was interpreted to be an intermediate product of marine *Bacillus* sp. Strain SG-1. Mandernack et al. (1995) concluded that Mn(II) is oxidized directly to Mn(IV) without an intermediate phase. Webb et al. (2005) synthesized a Mn-phase primarily as disordered hexagonal birnessite, which transformed after a few days to a pseudo-orthogonal birnessite. These Mn oxides differ slightly from the disordered, hexagonal phyllomanganates of manganese nodules from the CCZ. In contrast, Villalobos et al. (2003) determined a $\sim 7\text{\AA}$ hexagonal phyllomanganate produced by *Pseudomonas putida*. Furthermore, Hastings and Emerson (1986) and Bargar et al. (2005) showed that bacterial Mn(II) oxidation leads to the production of X-ray amorphous Mn oxides similar to $\delta\text{-MnO}_2$ of natural Mn-Fe encrustations. The authors suggest that these Mn oxides are the primary biominerals that are reworked through abiotic processes to become more stable and crystalline Mn oxides such as 10\AA phyllomanganates.

Microbially mediated Mn^{2+} oxidation is faster by several orders of magnitude than abiotic oxidation (Villalobos et al. 2003; Morgan 2005; Tebo et al. 2005, 2007). However, the turnover rates of abiotic oxidation correspond much better to the general growth rates of Mn nodules of up to a few tens of mm per million years (Lyle 1982; Halbach et al. 1988; Eisenhauer et al. 1992; Bollhöfer et al. 1996; Han et al. 2003).

Thus, in summary, the occurrence of bacteria in manganese nodules is recognized and there is a general understanding that their activity may influence the formation of manganese oxide minerals. However, whether microbial activity just modifies Mn nodules or whether their activity is essential for nodule formation is still a matter of debate.

2.4.4 Hydrothermal Precipitation

As Mn^{2+} is soluble under reducing and acid conditions, and as its solubility is not temperature-dependent, Mn^{2+} can not only be transported by hydrothermal solutions but also remains dissolved until hydrothermal fluids are oxidized upon contact with oxic seawater. Therefore, Mn^{2+} is enriched in low-temperature hydrothermal

fluids which occur either at the periphery of an active high-temperature hydrothermal vent field or during the waning stage of a hydrothermal system. Manganese will be oxidized and will precipitate as Mn oxide (mainly todorokite) upon mixing of these fluids with cold, oxic seawater, forming manganese crusts or irregularly shaped precipitates within or at the seafloor (Hein et al. 1990; Rogers et al. 2001; Kuhn et al. 2003).

Manganese is also enriched in high-temperature, black smoker fluid emanating from hydrothermal systems into the water column and forming hydrothermal plumes (Lilley et al. 1995). Hydrothermal plumes develop as a layer in the oceanic water column about 100–400 m above the seafloor and drift away from the hydrothermal system due to the activity of near-bottom currents. Manganese (and Fe) is oxidized during the horizontal drift of the hydrothermal plume, forming Mn-Fe-rich plume fallout which can either generate hydrothermal Fe-Mn crusts on rock outcrops or can contribute to a Fe-Mn oxide component of deep-sea sediments (Kuhn et al. 1998, 2000).

Manganese oxide precipitates occur in every marine hydrothermal system worldwide. However, they play no economic role in modern marine systems. In contrast, the largest terrestrial Mn deposit, the giant Proterozoic Kalahari Manganese Field of South Africa containing 77% of all land-based Mn reserves, was formed as fallout from hydrothermal plumes (Cairncross and Beukes 2013).

2.5 Occurrence of Manganese Nodules

Manganese nodules occur in the abyssal plains of all major oceans in ~4000–6000 m water depth. However, Mn nodule fields of economic importance are only known from the Clarion-Clipperton Zone, the Central Indian Ocean Basin, and the Cook Islands area (Fig. 2.16). In these regions and in the Peru Basin, manganese nodule exploration has taken place since more than 30 years.

2.5.1 Clarion-Clipperton Zone

The *Clarion-Clipperton Zone* (CCZ) is the region with the largest contiguous occurrence of Mn nodule fields. It covers an area of about four million square kilometers which almost equals the size of the European Union (ISA 2010). The CCZ is located in the Central Pacific just north of the equator between Hawaii and Mexico (Fig. 2.16). The nodules are mixtures of hydrogenetic and diagenetic endmembers with an average diagenetic proportion of ~80% in the eastern CCZ and a continuously increasing hydrogenetic proportion towards the central and western CCZ. This leads to slightly increased cobalt and rare earth element contents in nodules from the central and western CCZ (Table 2.1). Apart from these slight changes, the chemical composition of the nodules is relatively constant throughout the whole CCZ, especially

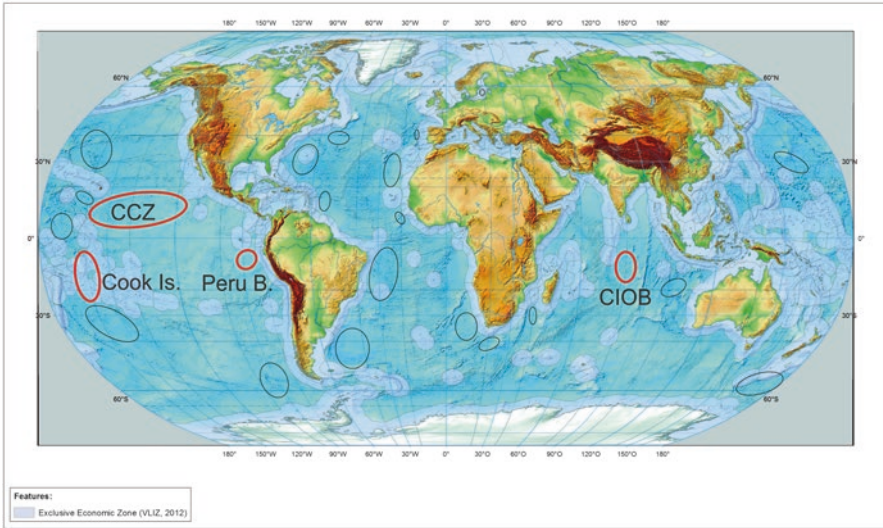


Fig. 2.16 Global occurrence of manganese nodule fields in abyssal plains of the world oceans. Areas marked in *red* are economically important regions and are discussed in the text. Manganese nodules occur in significant abundance in the remaining marked areas. However, they are also found elsewhere in abyssal plains of the world oceans but with lower abundance. *CCZ* Clarion-Clipperton Zone, *Cook Is.* Cook Islands (including the Penrhyn Basin and Manihiki Plateau), *Peru B.* Peru Basin, *CIOB* Central Indian Ocean Basin (figure adapted after Hein et al. 2013; background map from ESRI)

when compared to variations in nodule abundance (in kg/m^2). For instance, the coefficient of variation (CoV) of nodule composition in the eastern CCZ is less than 10% whereas that for nodule abundance is $>30\%$ (unpublished BGR data). Manganese nodule fields are not equally distributed on the seafloor within the CCZ but occur in patches. Economically interesting “patches” can cover an area of several thousand square kilometers.

Nodule abundance in the CCZ ranges between 0 and $\sim 30 \text{ kg/m}^2$ (based on wet nodule weight) with an average of 15 kg/m^2 (SPC 2013). The total amount of manganese nodules within the CCZ is estimated to be ca. 21 billion tons, which amounts to ca. 6 billion tons of manganese (Table 2.4; Visbeck and Gelpke 2014). The total Mn tonnage of CCZ nodules equals the global Mn reserves on land and total estimated tonnages of Ni, Co, Y, and Ti exceed those of land-based reserves by several factors (Table 2.4). Thus, manganese nodule mining could have a significant effect on the global production of certain metals and hence, on the global prices for those metals. However, one Mn nodule mining project with an annual production of two million tons of dry nodules would have only a small share in the global production of the main metals, except for the rare earth elements (Table 2.5). If five nodule mining projects would run simultaneously, the global share would be medium for cobalt and manganese; low for nickel, molybdenum, and lithium; and insignificant for copper. However, it would be very high for the rare earth elements (Table 2.5).

Table 2.4 Metal contents (in Mio. tons) of manganese nodules from the CCZ compared to land-based reserves and resources^a

Element	Clarion-Clipperton zone (CCZ)	Global reserves and resources on land ^b	Global reserves on land
Manganese (Mn)	5992	5200	630
Copper (Cu)	226	1000+	690
Titanium (Ti)	67	899	414
Rare earth oxides	15	150	110
Nickel (Ni)	274	150	80
Vanadium (V)	9.4	38	14
Molybdenum (Mo)	12	19	10
Lithium (Li)	2.8	14	13
Cobalt (Co)	44	13	7.5
Tungsten (W)	1.3	6.3	3.1
Niobium (Nb)	0.46	3	3
Arsenic (As)	1.4	1.6	1
Thorium (Th)	0.32	1.2	1.2
Bismuth (Bi)	0.18	0.7	0.3
Yttrium (Y)	2	0.5	0.5
Platinum group metals	0.003	0.08	0.07
Tellurium (Te)	0.08	0.05	0.02
Thallium (Tl)	4.2	0.0007	0.0004

^aData from Visbeck and Gelpke (2014)^bEconomically recoverable and sub-economic reserves**Table 2.5** Comparison between annual production of metals from nodule mining in the CCZ and the global annual metal production on land

Metal	Global annual terrestrial production (tons) ^a	Annual production of 1 nodule mining project (tons) ^b	Percentage of global annual production (%)	Annual production of 5 nodule mining projects (tons) ^b	Percentage of global annual production (%)
Cobalt	110,000	3400	3.1	17,000	15
Manganese	17,284,210	600,000	3.5	3,000,000	17
Copper	15,997,172	23,600	0.15	118,000	0.7
Nickel	1,786,300	27,800	1.6	139,000	7.8
Molybdenum	250,314	1200	0.48	6000	2.4
Lithium	62,231	280	0.45	1400	2.2
REO ^c	115,850	12,000	10	60,000	52

^aEU Report on Critical Raw Materials (2014)^bBased on annual production of 2 Mio. tons of dry nodules and the following average metal content of nodules: 0.17% Co, 30% Mn, 1.18% Cu, 1.39% Ni, 0.06% Mo, 0.014% Li, 0.6% REO^cRare earth element oxides

2.5.2 *Peru Basin*

The *Peru Basin* is located about 3000 km off the coast of Peru and covers about half of the size of the CCZ. A relatively high bioproductivity in the ocean's surface layer and the associated high flux of organic carbon to the seafloor explain the occurrence of an oxic-suboxic front at 10 cm sediment depth in the Peru Basin, this front separating soft oxic surface sediments from stiffer, suboxic sediments (von Stackelberg 1997). The average manganese nodule abundance is 10 kg/m² (Visbeck and Gelpke 2014), but maximum abundances of 50 kg/m² can be found at locations close to the carbonate compensation depth (CCD) at 4250 m water depth (von Stackelberg 1997). A significant difference to the CCZ is that most parts of the Peru Basin lie close to or above the CCD, leading to a significant carbonate content of up to 50% in the sediments (Koschinsky 2001). In contrast, CCZ surface sediments are almost devoid of carbonate (usually <1%) and consist of a mixture of siliceous ooze and deep-sea clay (ISA 2010).

Manganese nodules of the Peru Basin have similar nickel and molybdenum, distinctly lower copper, cobalt, and REY, but higher lithium contents and higher Mn/Fe ratios than CCZ nodules (Table 2.1). In terms of mineralogy, a recent study has shown that Peru Basin and CCZ surface nodules contain the same types of disordered phyllomanganates, and that todorokite is not a main mineralogical component (Wegorzewski et al. 2015).

The difference in metal content of nodules from the Peru Basin as compared to those of the CCZ can be attributed to a higher contribution of suboxic-diagenetic layers and a distinctly lower percentage of hydrogenetic layers in nodules from the Peru Basin (Wegorzewski and Kuhn 2014).

2.5.3 *Cook Islands*

The *Cook Islands Exclusive Economic Zone* covers about two million km² and includes the Penrhyn and Samoa Basin abyssal plains in the SW Pacific (Fig. 2.16). The seafloor of these plains is usually deeper than 4700 m and the sediments are mainly composed of zeolite-rich, pelagic-brown clays containing minor amounts of volcanic glass, iron and manganese oxides, phosphate debris as well as biogenic carbonate and silica in places (Cronan et al. 2010; Hein et al. 2015). The area is characterized by low sedimentation rates, low fluxes of organic matter, an abundant supply of nucleus material, and strong bottom currents. Evidently, these environmental conditions have remained fairly constant over a long period of time and have caused persistent oxic conditions at the seafloor and within the sediments, leading to the formation of slow-growing (mean 1.9 mm/Myr) hydrogenetic ferromanganese nodules with Mn/Fe ratios around unity (Table 2.1; Hein et al. 2015). Therefore, the nodules contain high amounts of cobalt (0.41%), titanium (1.20%), REY (0.17%),

and zirconium (524 $\mu\text{g/g}$), but they are low in nickel (0.38%), copper (0.23%), and manganese (16.1%) when compared to CCZ nodules (Table 2.1). Nodule abundances have been investigated in areas of potential exploration and range between 19 and 45 kg/m^2 , with a maximum of 58 kg/m^2 in small isolated areas. The relatively high nodule abundance together with elevated contents of high-tech metals (REY, Co, Ti) leads to the value of 1 ton of Cook Islands nodules being similar to the value of 1 ton of CCZ nodules at current metal prices (Hein et al. 2015).

2.5.4 *Central Indian Ocean Basin*

Within the *Central Indian Ocean Basin* (CIOB), economically interesting contiguous nodule fields occur in an area between 10°S and 16°30'S and 72°E and 80°E, in water depths between 3000 and 6000 m covering about 700,000 km^2 . Within this region, a nodule-rich area called the Indian Ocean Nodule Field (IONF) was delineated which covers ca. 300,000 km^2 (Mukhopadhyay et al. 2008; Mukhopadhyay and Ghosh 2010). The total manganese nodules in the IONF amount to about 1400 million tons with an average abundance of 4.5 kg/m^2 and 21.84 million tons of Ni + Cu + Co resources. However, nodule abundance is more variable and inhomogeneous than is the case in other nodule areas. Furthermore, there seems to be a relationship between the number of seamounts and faults and nodule abundance. Seamounts with heights >500 m and fault systems apparently increase the availability of nucleus material and thus the number and mass of nodules (Mukhopadhyay et al. 2008). The IONF consists of different sectors and the mode of nodule formation varies slightly between these sectors, leading to varying Mn/Fe ratios between 1.8 and 4.8, and a Ni + Cu + Co content ranging between 2.48 and 2.53%.

The mineralogical composition ranges from vernadite over birnessite to todorokite (Mukhopadhyay and Ghosh 2010). These results indicate that the nodules are mainly a mixture of variable proportions of diagenetic and hydroge-netic phases. The deep-sea sediments of the different IONF sectors consist of siliceous ooze, terrigenous material and pelagic red clays in variable amounts. Sedimentation rates decrease from 9 mm/kyr in the northern IONF to 1 mm/kyr in the south (Borole 1993). Apart from the Ni + Cu + Co contents of IONF nodules which are similar to those of CCZ nodules, IONF nodules have higher concentrations of lead and the rare earth elements (Table 2.1). The chemical and mineralogical compositions of nodules as well as the characteristics of the sedimentary environment indicate that IONF nodules are formed by the same hydro-genetic and diagenetic processes as CCZ nodules. The main difference between both areas is the nodule abundance, which is significantly higher in the CCZ. This might be attributed (1) to the lower sedimentation rates in the IONF, which have led to the formation of a higher proportion of hydrogenetic phases in the nodules,

and (2) to a higher input of terrigenous material, which reduces the supply of metals to the seafloor that can ultimately be mobilized into the nodules during early diagenesis. Nevertheless, given the large area and the available mining technology, a mining operation within the IONF is considered to be economic (Mukhopadhyay et al. 2008).

2.5.5 Other Ocean Areas

Apart from the abovementioned four areas which have been the target of nodule exploration for several decades, there are many other locations in the world oceans where manganese nodules occur (Fig. 2.16). Additional promising areas for investigation could be the abyssal plains in the Atlantic Ocean, which have been omitted from intense exploration so far. Another important but special region in terms of Mn nodule formation is the Baltic Sea with its fast growing ($0.013\text{--}1\text{ mm year}^{-1}$) diagenetic nodules at several locations. Relatively high nodule abundances between 10 and 40 kg/m^2 occur in the Gulfs of Riga, Finland, and Bothnia in water depths between a few tens of meters and about 150 m, covering areas of a few hundred km^2 . In the Russian sector of the Gulf of Finland, the nodule reserves amount to ca. six million tons and despite low trace metal contents ($<0.05\%$ for $\text{Co} + \text{Cu} + \text{Ni} + \text{Zn}$; Glasby et al. 1997), these nodules have already been commercially mined between 2004 and 2007 (Cherkashov et al. 2013).

Manganese nodules and other ferromanganese precipitates of special formation and metal content have been reported from the Gulf of Cadiz and the Galicia Bank offshore Spain (González et al. 2012, 2014). Their unusual metal composition (e.g., up to 1.8% Co and $>40\%$ Mn) is probably related to special local conditions, such as the activity of hydrocarbons or fault systems which may tap deeper crustal reservoirs.

References

- Bargar JR, Tebo BM, Bergmann U, Webb SM, Glatzel P, Chiu VQ, Villalobos M (2005) Biotic and abiotic products of Mn(II) oxidation by spores of the marine *Bacillus* sp. strain SG-1. *Am Mineral* 90:143–154
- Beiersdorf H (2003) Scientific challenges related to the development of a geological model for the manganese nodule occurrences in the clarion-clipperton zone (Equatorial North Pacific Ocean). In: Establishment of a geological model of polymetallic deposits in the Clarion-Clipperton Fracture Zone of the equatorial North Pacific Ocean. International Seabed Authority (ISA), Kingston, pp 175–200
- Blöthe M, Węgorzewski AV, Müller C, Simon F, Kuhn T, Schippers A (2015) Manganese-cycling microbial communities inside deep-sea manganese nodules. *Environ Sci Technol* 49:7692–7700

- Bodeř S, Manceau A, Geoffroy N, Baronnet A, Buatier M (2007) Formation of todorokite from vernadite in Ni-rich hemipelagic sediments. *Geochim Cosmochim Acta* 71:5698–5716
- Bollhöfer A, Eisenhauer A, Frank N, Pech D, Mangini A (1996) Thorium and uranium isotopes in a manganese nodule from the Peru basin determined by alpha spectrometry and thermal ionization mass spectrometry (TIMS): are manganese supply and growth related to climate? *Geologische Rundschau* 85:577–585
- Bonatti E, Kraemer T, Rydell H (1972) Classification and genesis of submarine iron-manganese deposits. In: Horn DR (ed) *Ferromanganese deposits on the ocean floor*. NSF, Washington, pp 149–166
- Borole DV (1993) Late Pleistocene sedimentation: a case study in the central Indian Ocean Basin. *Deep Sea Res* 40:761–775
- Bradt Miller LI, Anderson RF, Sachs JP, Fleisher MQ (2010) A deep respired carbon pool in the glacial equatorial Pacific Ocean. *Earth Planet Sci Lett* 299:417–425
- Bruland KW (1983) Trace elements in sea water. In: Riley JP, Chester R (eds) *Chemical oceanography*, vol 8. Academic Press, London, pp 156–220
- Burns RG, Burns VM (1977) Mineralogy. In: Glasby GP (ed) *Marine manganese deposits*. Elsevier oceanography series, vol 15. Elsevier, Amsterdam, pp 185–248
- Burns VM, Burns RG (1978) Authigenic todorokite and phillipsite inside deep sea manganese nodules. *Am Mineral* 63:827–831
- Burns RG, Burns VM, Stockman HW (1983). A review of the todorokite-buserite problem: implications to the mineralogy of marine manganese nodules. *Am Mineral* 68:972–980
- Byrne RH (2002) Speciation in seawater. In: Ure AM, Davidson CM (eds) *Chemical speciation in the environment*. Blackwell Publishing Ltd, Oxford, pp 322–357
- Cairncross B, Beukes NJ (2013) *The Kalahari Manganese Field*. Struik Nature Ltd., Cape Town, 383 p
- Cherkashov G, Smyslov A, Soreide F (2013) Fe-Mn nodules of the finnish bay (Baltic Sea): exploration and exploitation experience. In: Morgan CL (ed) *Recent developments in Atlantic seabed minerals exploration and other topics of timely interest*. The Underwater Mining Institute, Rio de Janeiro, 4 p
- Chester R, Jickells T (2012) *Marine geochemistry*, 3rd ed. Wiley-Blackwell, Oxford, 411 p
- Chukhrov FV, Gorshkov AI, Beresovskaya VV, Sivtsov AV (1979) Contributions to the mineralogy of authigenic manganese phases from marine manganese deposits. *Miner Deposita* 14:249–261
- Cronan DS, Rothwell G, Croudace I (2010) An ITRAX geochemical study of ferromanganiferous sediments from the Penrhyn Basin, South Pacific Ocean. *Mar Georesour Geotechnol* 28:207–221
- Drits VA, Tchoubar C (1990) X-ray diffraction by disordered lamellar structures: theory and applications to microdivided silicates and carbons. Springer, Berlin, p 371
- Drits VA, Silvester E, Gorshkov AI, Manceau A (1997) Structure of synthetic monoclinic Na-rich birnessite and hexagonal birnessite: I. Results from X-ray diffraction and selected-area electron diffraction. *Am Mineral* 82:946–961
- Drits VA, Lanson B, Gaillot AC (2007) Birnessite polytype systematics and identification by powder X-ray diffraction. *Am Mineral* 92:771–788
- Ehrlich HL (1963) Bacteriology of manganese nodules: I. Bacterial action on manganese in nodules enrichments. *Appl Microbiol* 11:15–19
- Ehrlich HL (1972) Response of some activities of ferromanganese nodule bacteria to hydrostatic pressure. In: Cilwell RR, Morita RY (eds) *Effect of the ocean environment on microbial activities*. University Park Press, Baltimore, pp 208–211
- Ehrlich HL (2000) Ocean manganese nodules: biogenesis and bioleaching possibilities. *Miner Metall Process* 17:121–128
- Ehrlich HL, Newman DK (2009) *Geomicrobiology*, 5th edn. CRC/Taylor & Francis Group, Boca Raton, p 606

- Eisenhauer A, Gögen K, Pernicka E, Mangini A (1992) Climatic influences on the growth rates of Mn crusts during the Late Quaternary. *Earth Planet Sci Lett* 109:25–36
- Froelich PN, Klinkhammer GP, Bender ML, Luedtke NA, Cullen D, Dauphin P (1979) Early oxidation of organic matter in pelagic sediments of the eastern equatorial Atlantic: suboxic diagenesis. *Geochim Cosmochim Acta* 43:1075–1090
- Galoway F, Bender M (1982) Diagenetic models of interstitial nitrate profiles in deep-sea suboxic sediments. *Limnol Oceanogr* 27:624–638
- Giovanoli R, Bürki P, Giuffredi M, Stumm W (1975) Layer structured manganese oxide-hydroxides. IV. The busenite group: structure stabilisation by transition elements. *Chimia* 29:517–520
- Giovanoli R (1980) On natural and synthetic manganese nodules. *Geol Geochem Manganese* 1(65):100–202
- Glasby GP (2006) Manganese: predominant role of nodules and crusts. In: Schulz HD, Zabel M (eds) *Marine geochemistry*. Springer, Heidelberg, pp 371–428
- Glasby GP, Emelyanov EM, Zhamoïda VA, Baturin GN, Leipe T, Bahlo R and Bonacker P (1997) Environments of formation of ferromanganese concretions in the Baltic Sea: a critical review. In: Nickelson K, Hein JR, Bühn B, Dasgupta S (eds) *Manganese mineralization: geochemistry and mineralogy of terrestrial and marine deposits*. Geol. Soc. Spec. Publ. No. 119, pp 213–238
- Golden DC, Dixon JB, Chen CC (1986) Ion exchange, thermal transformations, and oxidizing properties of birnessite. *Clays Clay Miner* 34:511–520
- González FJ, Somoza L, Leon R, Medialdea T, de Torres T, Ortiz JE, Lunar R, Martínez-Frías J, Merinero R (2012) Ferromanganese nodules and micro-hardgrounds associated with the Cadiz Contourite Channel (NE Atlantic): palaeoenvironmental records of fluid venting and bottom currents. *Chem Geol* 310–311:56–78
- González J, Somoza L, Lunar R, Martínez-Frías J, Medialdea T, León R, Martín-Rubí JA, Torres T, Ortiz JE, Marino E (2014) Polymetallic ferromanganese deposits research on the Atlantic Spanish continental margin. In: Hein JR, Barriga FJAS, Morgan, CL (eds) *Harvesting seabed minerals resources in harmony with nature*. UMI, Lisbon, Portugal
- Grangeon S, Lanson B, Miyata N, Tani Y, Manceau A (2010) Structure of nanocrystalline phyllo-manganates produced by freshwater fungi. *Am Mineral* 95:1608–1616
- Haeckel M, König I, Riech V, Weber ME, Suess E (2001) Pore water profiles and numerical modelling of biogeochemical processes in Peru Basin deep-sea sediments. *Deep Sea Res II* 48:3713–3736
- Halbach P, Friedrich G, von Stackelberg U (1988) The manganese nodule belt of the Pacific Ocean. Enke, Stuttgart, p 254
- Han X, Jin X, Yang S, Fietzke J, Eisenhauer A (2003) Rhythmic growth of Pacific ferromanganese nodules and their Milankovitch climatic origin. *Earth Planet Sci Lett* 211:143–157
- Hastings D, Emerson S (1986) Oxidation of manganese by spores of a marine *Bacillus*: kinetic and thermodynamic considerations. *Geochim Cosmochim Acta* 50(8):1819–1824
- Hein JR, Koschinsky A (2013) Deep-ocean ferromanganese crust and nodules. In: Holland H, Turekian K (eds) *Earth systems and environmental sciences, treatise on geochemistry*, 2nd edn. Elsevier, Amsterdam, pp 273–291
- Hein JR, Schulz MS, Kang J-K (1990) Insular and submarine ferromanganese mineralization of the Tonga-Lau region. *Mar Mining* 9:305–354
- Hein JR, Conrad TA, Staudigel H (2010) Seamount mineral deposits. A source of rare metals for high-technology industries. *Oceanography* 23(1):184–189
- Hein JR, Mizell K, Koschinsky A, Conrad TA (2013) Deep-ocean mineral deposits as a source of critical metals for high- and green-technology applications: comparison with land-based resources. *Ore Geol Rev* 51:1–14
- Hein JR, Spinardi F, Okamoto N, Mizell K, Thorburn D, Tawake A (2015) Critical metals in manganese nodules from the Cook Islands EEZ, abundances and distributions. *Ore Geol Rev* 68:97–116

- Herguera JC (2000) Last glacial paleoproductivity patterns in the eastern equatorial Pacific: benthic foraminifera records. *Mar Micropaleontol* 40:259–275
- Hlawatsch S, Garbe-Schönberg CD, Lechtenberg F, Manceau A, Tamura N, Kulik DA, Kersten M (2002) Trace metal fluxes to ferromanganese nodules from the western Baltic Sea as a record for long-term environmental changes. *Chem Geol* 181:697–709
- ISA (2010) A geological model of polymetallic nodules in the Clarion-Clipperton Fracture Zone. International Seabed Authority Technical Study No. 6. Kingston, Jamaica, p 75
- Koschinsky A (2001) Heavy metal distributions in Peru Basin surface sediments in relation to historic, present and disturbed redox environments. *Deep Sea Res II* 48:3757–3777
- Koschinsky A, Halbach P (1995) Sequential leaching of marine ferromanganese precipitates: genetic implications. *Geochim Cosmochim Acta* 59:5113–5132
- Koschinsky A, Hein JR (2003) Uptake of elements from seawater by ferromanganese crusts: solid-phase associations and seawater speciation. *Mar Geol* 198:331–351
- Krapf E (2014) Investigations of growth structures of manganese nodules from the East Pacific using micro-analytical approaches. Master thesis (in German), University of Clausthal, Clausthal-Zellerfeld, p 62
- Kuhn T, Bau M, Blum N, Halbach P (1998) Origin of negative Ce anomalies in mixed hydrothermal-hydrogenetic Fe–Mn crusts from the Central Indian Ridge. *Earth Planet Sci Lett* 163:207–220
- Kuhn T, Burger H, Castradori D, Halbach P (2000) Tectonic and hydrothermal evolution of ridge segments near the Rodrigues Triple Junction (Central Indian Ocean) deduced from sediment geochemistry. *Mar Geol* 169:391–409
- Kuhn T, Bostick BC, Koschinsky A, Halbach P, Fendorf S (2003) Enrichment of Mo in hydrothermal Mn precipitates: possible Mo sources, formation process and phase associations. *Chem Geol* 199:29–43
- Lilley MD, Feely RA, Trefry JH (1995) Chemical and biochemical transformations in hydrothermal plumes. In: Humphris SE, Zierenberg RA, Mullineaux LS, Thomson RE (eds) *Seafloor hydrothermal systems*. Geophys. Monogr. 91, Am. Geophys. Union, Washington, pp 369–391
- Lyle M (1982) Estimating growth rates of ferromanganese nodules from chemical compositions: implications for nodule formation processes. *Geochim Cosmochim Acta* 46(11):2301–2306
- Manceau A, Gorshkov AI, Drits VA (1992a) Structural chemistry of Mn, Fe, Co, and Ni in manganese hydrous oxides: Part II. Information from EXAFS spectroscopy and electron and X-ray diffraction. *Am Mineral* 77:1144–1157
- Manceau A, Gorshkov AI, Drits VA (1992b) Structural chemistry of Mn, Fe, Co, and Ni in manganese hydrous oxides: Part I. Information from XANES spectroscopy. *Am Mineral* 77:113–1143
- Manceau A, Drits VA, Silvester E, Bartoli C, Lanson B (1997) Structural mechanism of Co^{2+} oxidation by the phylломanganate buserite. *Am Mineral* 82(11–12):1150–1175
- Manceau A, Marcus MA, Grangeon S (2012) Determination of Mn valence states in mixed-valent manganates by XANES spectroscopy. *Am Mineral* 97:816–827
- Manceau A, Lanson M, Takahashi Y (2014) Mineralogy and crystal chemistry of Mn, Fe, Co, Ni, and Cu in a deep-sea Pacific polymetallic nodule. *Am Mineral* 99:2068–2083
- Mandernack KW, Post J, Tebo BM (1995) Manganese mineral formation by bacterial spores of the marine *Bacillus*, strain SG-1: evidence for the direct oxidation of Mn(II) to Mn(IV). *Geochim Cosmochim Acta* 59:4393–4408
- Mann S, Sparks NHC, Scott GHE, deVrind-deJong EW (1988) Oxidation of manganese and formation of Mn_2O_4 (hausmannite) by spore coats of a marine *Bacillus* sp. *Appl Environ Microbiol* 54:2140–2143
- McLennan SM (1989) Rare earth elements in sedimentary rocks: influence of provenance and sedimentary processes. In: Lipin BR, McKay GA (eds) *Geochemistry and mineralogy of rare earth elements*. *Rev. Mineral.* 21, Mineral. Soc. Am., Washington, pp 169–200
- Mewes K, Mogollón JM, Picard A, Rühlemann C, Kuhn T, Nöthen K, Kasten S (2014) The impact of depositional and biogeochemical processes on small scale variations in nodule abundance in the Clarion–Clipperton Fracture Zone. *Deep-Sea Res* 191:125–141

- Miyata N, Maruo K, Tani Y, Tsuno H, Seyama H, Soma M, Iwahori K (2006) Production of biogenic manganese oxides by anamorphic ascomycete fungi isolated from streambed pebbles. *Geomicrobiol J* 23:63–73
- Morgan JJ (2005) Kinetics of reaction between O_2 and Mn (II) species in aqueous solutions. *Geochim Cosmochim Acta* 69:35–48
- Mukhopadhyay R, Ghosh AK (2010) Dynamics of formation of ferromanganese nodules in the Indian Ocean. *J Asian Earth Sci* 37:394–398
- Mukhopadhyay R, Ghosh AK, Iyer SD (2008) The Indian Ocean nodule field. Geology and resource potential. In: Hale M (series editor) *Handbook of exploration and environmental geochemistry* no. 10. Elsevier, Amsterdam, p 292
- Müller PJ, Hartmann M, Suess E (1988) The chemical environment of pelagic sediments. In: Halbach P, Friedrich G, von Stackelberg U (eds) *The manganese nodule belt of the Pacific ocean: geological, environment, nodule formation, and mining aspects*. Enke, Stuttgart, pp 70–90
- Novikov GV, Bogdanova O, Yu (2007) Transformations of ore minerals in genetically different oceanic ferromanganese rocks. *Lithol Miner Resour* 42:303–317
- Peacock CL, Sherman DM (2007a) Sorption of Ni by birnessite: equilibrium controls on Ni in seawater. *Chem Geol* 238:94–106
- Peacock CL, Sherman DM (2007b) Crystal-chemistry of Ni in marine ferromanganese crusts and nodules. *Am Mineral* 92:1087–1092
- Post JE, Appleman DE (1988) Chalcophanite, $ZnMn_3O_7 \cdot 3H_2O$: new crystal-structure determinations. *Am Mineral* 73:1401–1404
- Post JE, Appleman DE (1994) Crystal structure refinement of lithiophorite. *Am Mineral* 79:370–374
- Post JE, Bish DL (1988) Rietveld refinement of the todorokite structure. *Am Mineral* 73:861–869
- Post JE, Veblen DR (1990) Crystal structure determinations of synthetic sodium, magnesium, and potassium birnessite using TEM and the Rietveld method. *Am Mineral* 75:477–489
- Post JE, Heaney PJ, Hanson J (2003) Synchrotron X-ray diffraction of the structure and dehydration behavior of todorokite. *Am Mineral* 88:142–150
- Rogers TDS, Hodkinson RA, Cronan DS (2001) Hydrothermal manganese deposits from the Tonga-Kermadec Ridge and Lau Basin Region, Southwest Pacific. *Mar Geores Geotechnol* 19:245–268
- Rosson RA, Nealson KH (1982) Manganese bacteria and the marine manganese cycle. In: Ernst WG, Morin JG (eds) *The environment of the deep sea*. Prentice Hall Inc., Englewood Cliffs, pp 206–216
- Schweissfurth R (1971) Manganknollen im Meer. *Naturwissenschaften* 58:344–347
- Shaw TJ, Gieskes JM, Jahnke RA (1990) Early diagenesis in differing depositional environments: the response of transition metals in pore water. *Geochim Cosmochim Acta* 54:1233–1246
- SPC (2013) Deep sea minerals: manganese nodules, a physical, biological, environmental, and technical review. In: Baker E, Beaudoin Y (eds) vol 1B. *Secretariat of the Pacific Community*
- Stumm W, Morgan JJ (1981) *Aquatic chemistry: an introduction emphasizing chemical equilibria in natural waters*, 2nd edn. Wiley, New York, p 780
- Takahashi Y, Manceau A, Geoffroy N, Marcus MA, Usui A (2007) Chemical and structural control of the partitioning of Co, Ce, and Pb in marine ferromanganese oxides. *Geochim Cosmochim Acta* 71:984–1008
- Tebo BM, Bargar JR, Clement BG, Dick GJ, Murray KJ, Parker D, Webb SM (2004) Biogenic manganese oxides: properties and mechanisms of formation. *Annu Rev Earth Planet Sci* 32:287–328
- Tebo BM, Johnson HA, McCarthy JK, Templeton AS (2005) Geomicrobiology of manganese (II) oxidation. *Trends Microbiol* 13:421–428
- Tebo BM, Clement BG, Dick GJ (2007) Biotransformations of manganese. In: Hurst CJ, Crawford RL, Garland JL, Lipson DA, Mills AL, Stetzenbach LD (eds) *Manual of environmental microbiology*, 3rd edn. ASM Press, Washington, pp 1223–1238

- Turner S, Buseck PR (1979) Manganese oxide tunnel structures and their intergrowths. *Science* 203:456–458
- Usui A, Mita N (1995) Geochemistry and mineralogy of a modern buserite deposit from a hot spring in Hokkaido, Japan. *Clays Clay Miner* 43:116–127
- Usui A, Mellin TA, Nohara M, Yuasa M (1989) Structural stability of marine 10\AA manganates from the Ogasawara (Bonin) Arc: implication for low-temperature hydrothermal activity. *Mar Geol* 86:41–56
- Villalobos M, Toner B, Bargar J, Sposito G (2003) Characterization of the manganese oxide produced by *Pseudomonas putida* strain MnB1. *Geochim Cosmochim Acta* 67:2649–2662
- Visbeck M, Gelpke N (2014) World ocean review 3. Maribus gGmbH, Hamburg, p 163
- von Stackelberg, U. (1997). Growth history of manganese nodules and crusts of the Peru Basin. In: Manganese mineralization: geochemistry and mineralogy of terrestrial and marine deposits. *Geol Soc Spec Pub*, 119, pp 153–176
- von Stackelberg U (2000) Manganese nodules of the Peru Basin. In: Cronan DS (ed) *Handbook of marine mineral deposits*. CRC Press, Boca Raton, pp 197–238
- von Stackelberg U, Beiersdorf H (1987) Manganese nodules and sediments in the equatorial North Pacific Ocean, “Sonne” Cruise SO25, 1982. *Geol. Jahrb.*, D87:403 pp
- von Stackelberg U, Marchig V (1987) Manganese nodule from the equatorial North Pacific Ocean. *Geol Jahrb* D87:123–227
- Warren BE (1941) X-ray diffraction in random layer lattices. *Phys Rev* 59:693–698
- Webb SM, Tebo BM, Bargar JR (2005) Structural characterization of biogenic Mn oxides produced in seawater by the marine *Bacillus* sp. strain SG-1. *Am Mineral* 90:1342–1357
- Wegorzewski AV, Kuhn T (2014) The influence of suboxic diagenesis on the formation of manganese nodules in the Clarion Clipperton nodule belt of the Pacific Ocean. *Mar Geol* 357:123–138
- Wegorzewski A, Kuhn T, Dohrmann R, Wirth R, Grangeon S (2015) Mineralogical characterization of individual growth structures of Mn-nodules with different Ni+Cu content from the central Pacific Ocean. *Am Mineral* 100:2497–2508



Thomas Kuhn is a marine geologist at the German Federal Institute for Geosciences and Natural Resources (BGR). He has specialized in solid-phase associations and structural control of trace elements in ferromanganese precipitates, rocks, and sediments; the automated analysis of seafloor images; geostatistical resource estimation; and the analysis of hydro-acoustic data for the exploration of manganese nodule fields. He has participated in more than 25 research cruises to all major oceans.



Anna V. Wegorzewski is a marine geologist at the German Federal Institute for Geosciences and Natural Resources (BGR). She is working on the mineralogical composition of manganese nodules, especially on the enrichment and incorporation of economically interesting metals into the manganese phases particularly with regard to further metallurgical treatment. Since 2010, she participated in five research cruises in the Pacific and Indian ocean.



Carsten Rühlemann is a marine geologist at the German Federal Institute for Geosciences and Natural Resources (BGR) and is the project manager for the exploration of manganese nodules in the German license area. He has participated in more than 20 ocean-going expeditions.



Annemiek Vink is a marine bio-geologist at the German Federal Institute for Geosciences and Natural Resources (BGR). She is responsible for the coordination of the environmental management program in the German Mn-nodule exploration license area in the CCZ, which focuses strongly on the collection of adequate environmental baseline data as well as the analysis of potential impacts of Mn-nodule exploitation on faunal communities (e.g., due to nodule removal, sediment plume dispersion and settling). She has participated in several research/exploration cruises into the CCZ.

Deep-Sea Mining

Resource Potential, Technical and Environmental
Considerations

Sharma, R. (Ed.)

2017, X, 535 p. 270 illus., 131 illus. in color., Hardcover

ISBN: 978-3-319-52556-3